

SUPPORTING INFORMATION

Methane Adsorption on Heteroatom-Modified Maquettes of Porous Carbon Surfaces

Rylan Rowsey,¹ Erin E. Taylor,¹ Stephan Irle,² Nicholas P. Stadie,^{1*} and Robert K. Szilagyi^{1*}

¹Department of Chemistry & Biochemistry, Montana State University, Bozeman, Montana, 59717, United States

²Computational Sciences & Engineering Division, Oak Ridge National Laboratory, Oak Ridge, Tennessee, 37831, United States

* Corresponding authors: szilagyi@montana.edu and nstadie@montana.edu

Additional electronic supporting information including the atomic positional coordinates for all *maquettes*, templates for geometric and electronic structure analysis, formatted checkpoint files, and electron density and spin density cube files is available free of charge at Zenodo.org (DOI: 10.5281/zenodo.4898710 or URL: <https://zenodo.org/record/4898710>)

Table of Contents:

Figure S1.	Graphical illustrations of the nomenclature employed for adsorbent reference orientation and atom numbering. The central position 1 is the site of substitution (X1 position, X = C, B, or N). Relative to X1, the nearest neighbors (α positions) are numbered 2–4, the second-nearest neighbors (β positions) are numbered 5–10, and the third-nearest neighbors (γ positions) are numbered 11–13. The methyldene group carbon is numbered 14. While this is different from the IUPAC numbering convention, it is suited for clarity within the present work. The rings of the MPh models are labeled with roman numerals. Ring I contains the dangling methyldene group, which breaks the symmetry of the model. Rings II and III are adjacent and opposite to ring I, respectively. 6
Figure S2.	Graphical illustrations of the nomenclature employed for representative internal coordinates of the adsorbent. The “inner sphere” coordinates are defined by three C–C distances between the site of substitution (X1) and each of the α C atoms. The “outer sphere” is defined by six C–C distances between adjacent α C and β C atoms. The “peripheral sphere” is defined by six plus one C–C distances between adjacent β C and γ C atoms, and the methyldene γ C atom. The planarity of the molecule is described by the distance (δ) between the site of substitution (X1) and the plane formed by the ring centroids (X _I , X _{II} , and X _{III}). Finally, the out-of-plane wagging character of the methyldene group is defined by the angle (w) between the γ C... <i>ipso</i> - β C... <i>para</i> - α C of ring I. Notably, the in-plane bending of the MPh structure is typically negligible owing to the extensive π -conjugation of all carbon/heteroatom sites. 6
Figure S3.	Graphical illustrations of the nomenclature employed for adsorption model geometry, atom numbering, and internal coordinates. The bond length of the adsorption interaction is defined by the distance between the methane carbon (C25) and site of substitution (X1), as well as the three distances between the proximal H atoms of the methane molecule and the nearest ring centroids (H26...X _I , H27...X _{II} , and H28...X _{III}). The distortion imposed by the adsorption interaction is defined by four C–H distances within the methane (adsorbate) molecule, and the dihedral angles (ω _I , ω _{II} , and ω _{III}) between the methane C–H bonds and the closest ring centroid: C25–H(26,27,28)...X1... γ C(11,12,13). The C–H distances are further classified as proximal (C25–H26, C25–H27, and C25–H28) or distal (C25–H29) relative to the adsorbent surface. 7
Figure S4.	Top and side views of a larger “curved blade” <i>maquette</i> (XC ₄₇ H ₂₀) with fourteen possible sites of substitution (X = C, B, or N) for CH ₄ adsorption, shown in yellow. Only one of the fourteen sites is substituted with B or N in each calculation, the remainder remaining as C. 8
Figure S5.	(a) Potential energy surface maps for methane interactions with MPh and its heteroatom-substituted variants (B-MPh and N-MPh) in κ^1 approach geometry at the PBE/6-311++G** level. (b) The PBE optimized adsorption models MPh×CH ₄ , B-MPh×CH ₄ , and N-MPh×CH ₄ in their starting geometries used for structural optimizations. (c) Potential energy difference maps between the PBE/6-311++G** and the MN15/6-311++G** levels of theory. 9

Figure S6.	Comparison of the completeness of capturing electron correlation with the employed levels of correlated MO theory as a function of 6-311++G** (diamond), <i>aug-cc-pVDZ</i> (square), and <i>aug-cc-pVTZ</i> (star) basis sets for MPh (gray), B-MPh (salmon) and N-MPh (blue), for (a) the adsorbent models and (b) the adsorption models. The $1.2\pm 0.2\%$ shift between the two sets of curves and the identical trends (parallel lines within 2% variation) between the results with and without the triples substitution (T) allows for the extrapolation of the missing CCSD and CCSD(T) results for the <i>aug-cc-pVTZ</i> basis set.	10
Figure S7.	Electron density difference plots for methane interactions with MPh and its heteroatom-substituted variants: (a-c) at a high contour level of 5×10^{-4} (e^{-}) ² Å ⁻³ and (d-f) at a low contour level of 1.5×10^{-4} (e^{-}) ² Å ⁻³ for MPh×2CH ₄ (a,d), B-MPh×2CH ₄ (b,e), and N-MPh×2CH ₄ (c,f). Electron density difference between the double adsorption model and the separate adsorbent and adsorbates at the MN15/def2-QZVPP level is shown (positive difference in red, negative difference in blue). See Figure 3 for the corresponding single (n = 1) adsorption models.	11
Figure S8.	Comparison of the electron density of MPh and the spin density of B-MPh and N-MPh upon methane adsorption. (a) LUMO and (c) HOMO electron density contour plots for MPh×2CH ₄ at a contour level of 4.5×10^{-2} (e^{-}) ² Å ⁻³ and (b,d) spin density contour plots for N-MPh×2CH ₄ and B-MPh×2CH ₄ at a contour level of 3.5×10^{-3} (e^{-}) ² Å ⁻³ . See Figure 4 for the corresponding single (n = 1) adsorption models.	12
Figure S9.	Atomic spin density distribution analysis upon single (n = 1) and double (n = 2) methane adsorption on B-MPh (orange/red) and N-MPh (cyan/blue) determined by two conceptually different population analysis methods: (a) Hirshfeld (HPA) and (b) Weinhold (NPA), at the MN15/def2-QZVPP level of theory. See Figures S1-S3 for the atomic numbering and Tables S11-S12 for the tabulated data.	13
	<i>The figure is followed by a brief discussion about the effect and challenges of spin polarization due to the presence of an electron hole and extra electron in the S=1/2 paramagnetic [B-MPh] and [N-MPh] adsorbents; respectively, in comparison to the pure C, diamagnetic [MPh] adsorbent.</i>	
Figure S10.	Stationary structures of the two “curved blade” adsorption models (BC ₄₇ H ₂₀), where the CH ₄ adsorbate slipped to an adjacent adsorption site due to the curvature and distortion of the aromatic π-system. Optimization was performed at the MN15/6-31G* (MN15-) level.	15
Table S1:	Overview of literature examples of experimental (top) and theoretical (bottom) investigations of methane adsorption on carbon surfaces. The sign convention corresponds to energy of dissociation/desorption. All experimental and theoretical values refer to isosteric heat of desorption (q _{st}) from gas adsorption measurements and calculated desorption energy (Δ _{des} E) from quantum potential energy differences, respectively.	16
Table S2.	Graphical illustration and Z-matrix definitions for κ ¹ , μ ₂ , μ ₃ , and η ² approaches of CH ₄ to the X1 position of MPh and its heteroatom substituted variants.	17

Table S3.	Free adsorbent structures (LoT: MN15 using the STO-3G {MN15}, SDDAll [MN15], 6-31G* (MN15-), or def2-QZVPP (MN15+) basis sets) of MPh, B-MPh, and N-MPh as described by averages and standard deviations of inner, outer, and peripheral sphere C–C distances in Å, out-of-planarity (δ , in Å) of the site of substitution, and wagging angle (w , in degrees) of the methyldene group (see Table S4 for the geometry upon methane adsorption).....	18
Table S4.	Adsorbent structures upon adsorption (LoT: MN15, MP2, MP4 ^{SDQ} , or CCSD using the 6-311++G** basis set, or MN15 using the STO-3G {MN15}, SDDAll [MN15], 6-31G* (MN15-), or def2-QZVPP (MN15+) basis sets) of methane on MPh, B-MPh, and N-MPh, as described by averages and standard deviations of inner, outer, and peripheral sphere C–C distances in Å, out-of-planarity (δ , in Å) of the site of substitution, and wagging angle (w , in degrees) of the methyldene group (see Tables 1 and S3 for the free adsorbent structures).	19
Table S5.	Adsorption model structures (LoT: MN15 using the STO-3G {MN15}, SDDAll [MN15], 6-31G* (MN15-), or def2-QZVPP (MN15+) basis sets) of methane on MPh, B-MPh, and N-MPh. Adsorption by one ($n = 1$) and two ($n = 2$) methane molecules is described by interaction distances and twisting angles: methane to central site (C25...X1) distance, proximal H to closest ring centroid (H _p ...X _i) distance, dihedral angle formed by X _i ...X1...C25–H _p (ω), and proximal and distal C–H bond lengths.	20
Table S6.	Desorption energies (Δ_{des} , kJ mol ⁻¹) for MPh \times nCH ₄ \rightarrow MPh + nCH ₄ (LoT: MN15 using the STO-3G {MN15}, SDDAll [MN15], 6-31G* (MN15-), or def2-QZVPP (MN15+) basis sets). CBS refers to the modified complete basis set extrapolation method employing the CBS-QB3 formalism, but utilizing the MN15/6-311++G** geometry. The standard enthalpy, Gibbs free energy, and entropy of desorption are calculated at 298 K using a simple statistical mechanical model assuming ideal gas behavior. A modest statistical analysis (average and standard deviation) of the thermochemical quantities is shown, normalized per mole of CH ₄	21
Table S7.	Energy components of the modified CBS-QB3 method using fixed MN15/6-311++G** equilibrium structures for adsorbent, adsorbate, and adsorption models and corresponding vibrational analyses (invoking Gaussian keyword ‘StartMP2’ and using the results of the frequency calculation from the converged MN15 checkpoints).	22
Table S8.	Energy stabilization ($\Delta\Delta E^{\text{QM}}$) and desorption (\rightarrow MPh+CH ₄) energy differences (in kJ mol ⁻¹) due to optimizing the MN16/6-311++G** equilibrium structures of the adsorbent, adsorbate, and the adsorption model using a conceptually converging series of correlated MO theories (LoT: MP2, MP3, MP4, CCSD, or CCSD(T) using the 6-311++G** basis set).	24
Table S9.	Atomic charge (electron) distribution analysis upon single ($n = 1$) and double ($n = 2$) methane adsorption on MPh, B-MPh, and N-MPh determined by three conceptually different population analysis methods: Hirshfeld (HPA), Weinhold (NPA), and Merz-Kollman (ESP) at the MN15/def2-QZVPP level of theory. See Figure 2 for a graphical plot and Figure S1 for the numbering of atom positions.	25

Table S10.	Atomic charge (electron) distribution analysis upon single ($n = 1$) and double ($n = 2$) methane adsorption on MPh, B-MPh, and N-MPh determined by three conceptually different population analysis methods: Hirshfeld (HPA), Weinhold (NPA), and Merz-Kollman (ESP) at the MN15/def2-QZVPP level of theory. See Figure 2 for a graphical plot and Figure S1 for the numbering of atom positions (numbering of the second adsorbate is logical).	26
Table S11.	Atomic spin densities of the adsorbent molecule for single ($n = 1$) and double ($n = 2$) methane adsorption on B-MPh and N-MPh from Hirshfeld population analysis (HPA) and Weinhold natural population analysis (NPA) at the MN15/def2-QZVPP level of theory. See Figure S1 for the numbering of atom positions.	27
Table S12.	Atomic spin densities of the adsorbate molecule(s) for single ($n = 1$) and double ($n = 2$) methane adsorption on B-MPh and N-MPh from Hirshfeld population analysis (HPA) and Weinhold natural population analysis (NPA) at the MN15/def2-QZVPP level of theory. See Figure S1 for the numbering of atom positions (numbering of the second adsorbate is logical).	28
Table S13.	Thermochemical quantities (in kJ mol^{-1}) for comparison to experimental measurements of physisorptive binding of methane on porous carbon surfaces at 298 K. LoT: MN15/6-311++G**. MPh \times CH ₄ corresponds to 5.6 mmol g^{-1} of absolute uptake and MPh \times 2CH ₄ corresponds to 11.2 mmol g^{-1} , where uptake is defined as the true or “absolute” quantity. At room temperature (298 K), this corresponds to the following equilibrium pressures for adsorption on ZTC: 9.5 and 26.8 bar (or 9.3 and 26.4 atm), respectively. The enthalpy of desorption ($\Delta_{\text{des}}H$) at these conditions is measured to be 13.5 and 13.1 kJ mol^{-1} , respectively (Stadie et al., 2015 – Reference 49).	29
Table S14.	Thermochemical quantities (in kJ mol^{-1}) for comparison to experimental measurements of physisorptive binding of methane on porous carbon surfaces at 298 K. LoT: MN15/def2-QZVPP. MPh \times CH ₄ corresponds to 5.6 mmol g^{-1} of absolute uptake and MPh \times 2CH ₄ corresponds to 11.2 mmol g^{-1} , where uptake is defined as the true or “absolute” quantity. At room temperature (298 K), this corresponds to the following equilibrium pressures for adsorption on ZTC: 9.5 and 26.8 bar (or 9.3 and 26.4 atm), respectively. The enthalpy of desorption ($\Delta_{\text{des}}H$) at these conditions is measured to be 13.5 and 13.1 kJ mol^{-1} , respectively (Stadie et al., 2015 – Reference 49).	29
Table S15.	Consequences of the gradual relaxation of the XC ₄₇ H ₂₀ \times CH ₄ (i.e., blade \times CH ₄ or X-blade \times CH ₄ , X = B or N), adsorption model structures on CH ₄ binding energies in kJ mol^{-1} , as a function of site of interaction (C, B, or N). A number of stationary structures (N) below 28 indicates a ‘slip’ of CH ₄ into an adjacent adsorption site than originally targeted. Basis sets used for MN15-, MN15, and MN15 levels are 6-31G*, 6-311++G**, def2-QZVPP, respectively with the MN15 functional.	30

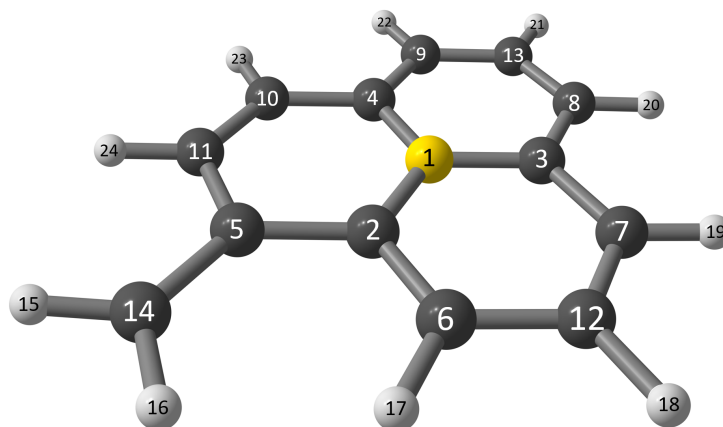


Figure S1. Graphical illustrations of the nomenclature employed for adsorbent reference orientation and atom numbering. The central position 1 is the site of substitution (X1 position, X = C, B, or N). Relative to X1, the nearest neighbors (α positions) are numbered 2–4, the second-nearest neighbors (β positions) are numbered 5–10, and the third-nearest neighbors (γ positions) are numbered 11–13. The methylidene group carbon is numbered 14. While this is different from the IUPAC numbering convention, it is suited for clarity within the present work. The rings of the MPh models are labeled with roman numerals. Ring I contains the dangling methylidene group, which breaks the symmetry of the model. Rings II and III are adjacent and opposite to ring I, respectively.

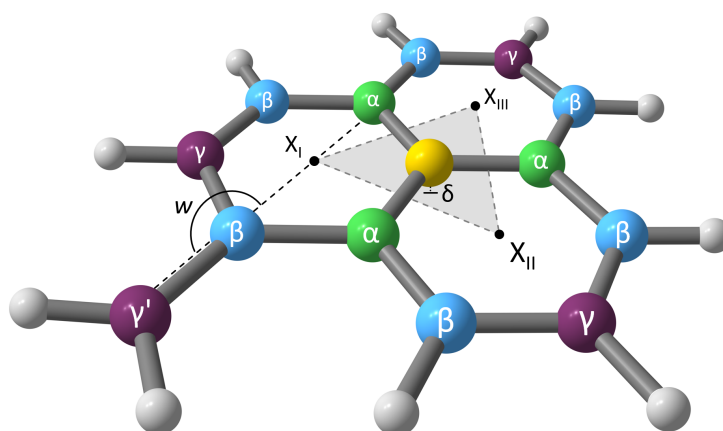


Figure S2. Graphical illustrations of the nomenclature employed for representative internal coordinates of the adsorbent. The “inner sphere” coordinates are defined by three C–C distances between the site of substitution (X1) and each of the α C atoms. The “outer sphere” is defined by six C–C distances between adjacent α C and β C atoms. The “peripheral sphere” is defined by six plus one C–C distances between adjacent β C and γ C atoms, and the methylidene γ' C atom. The planarity of the molecule is described by the distance (δ) between the site of substitution (X1) and the plane formed by the ring centroids (X_I , X_{II} , and X_{III}). Finally, the out-of-plane wagging character of the methylidene group is defined by the angle (w) between the γ' C...*ipso*- β C...*para*- α C of ring I. Notably, the in-plane bending of the MPh structure is typically negligible owing to the extensive π -conjugation of all carbon/heteroatom sites.

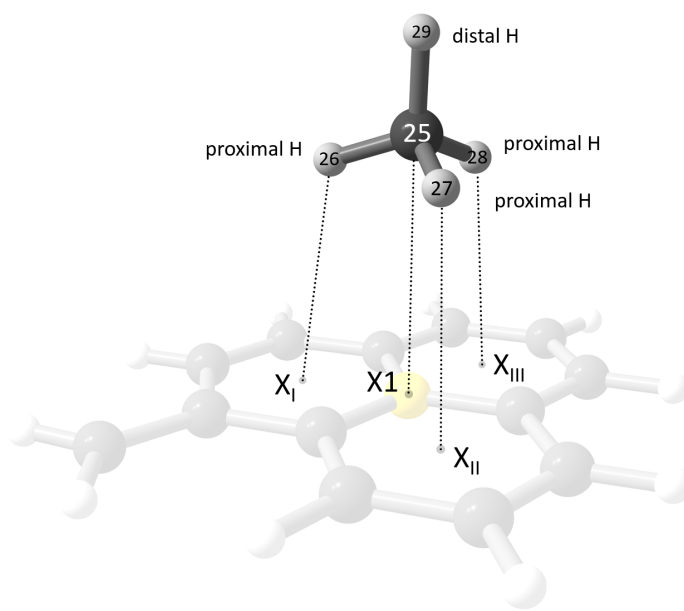


Figure S3. Graphical illustrations of the nomenclature employed for adsorption model geometry, atom numbering, and internal coordinates. The bond length of the adsorption interaction is defined by the distance between the methane carbon (C25) and site of substitution (X1), as well as the three distances between the proximal H atoms of the methane molecule and the nearest ring centroids (H26 \cdots X_I, H27 \cdots X_{II}, and H28 \cdots X_{III}). The distortion imposed by the adsorption interaction is defined by four C–H distances within the methane (adsorbate) molecule, and the dihedral angles (ω_I , ω_{II} , and ω_{III}) between the methane C–H bonds and the closest ring centroid: C25–H(26,27,28) \cdots X1 \cdots γ C(11,12,13). The C–H distances are further classified as proximal (C25–H26, C25–H27, and C25–H28) or distal (C25–H29) relative to the adsorbent surface.

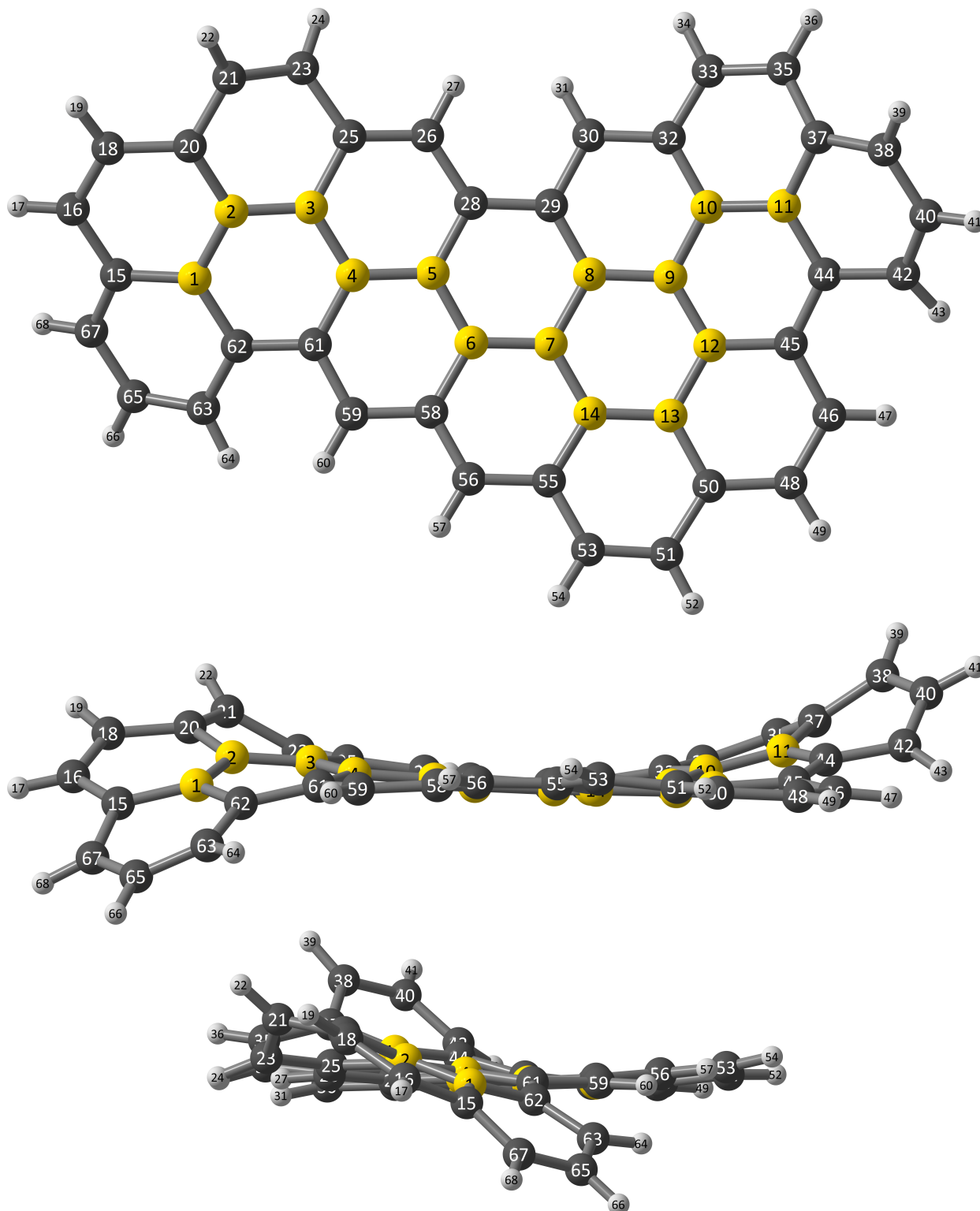


Figure S4. Top and side views of a larger “curved blade” *maquette* ($\text{XC}_{47}\text{H}_{20}$) with fourteen possible sites of substitution ($\text{X} = \text{C}, \text{B}, \text{or } \text{N}$) for CH_4 adsorption, shown in yellow. Only one of the fourteen sites is substituted with B or N in each calculation, the remainder remaining as C.

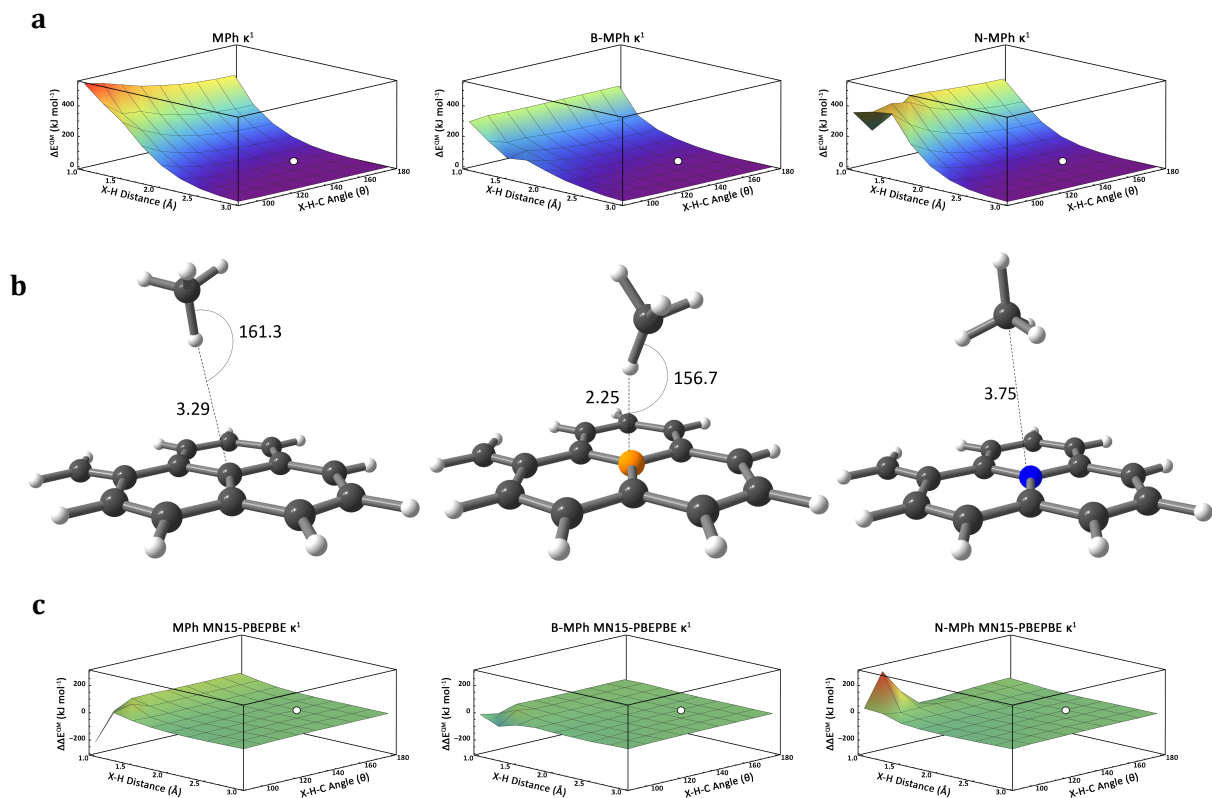


Figure S5. (a) Potential energy surface maps for methane interactions with MPh and its heteroatom-substituted variants (B-MPh and N-MPh) in κ^1 approach geometry at the PBE/6-311++G** level. (b) The PBE optimized adsorption models $\text{MPh} \times \text{CH}_4$, $\text{B-MPh} \times \text{CH}_4$, and $\text{N-MPh} \times \text{CH}_4$ in their starting geometries used for structural optimizations. (c) Potential energy difference maps between the PBE/6-311++G** and the MN15/6-311++G** levels of theory.

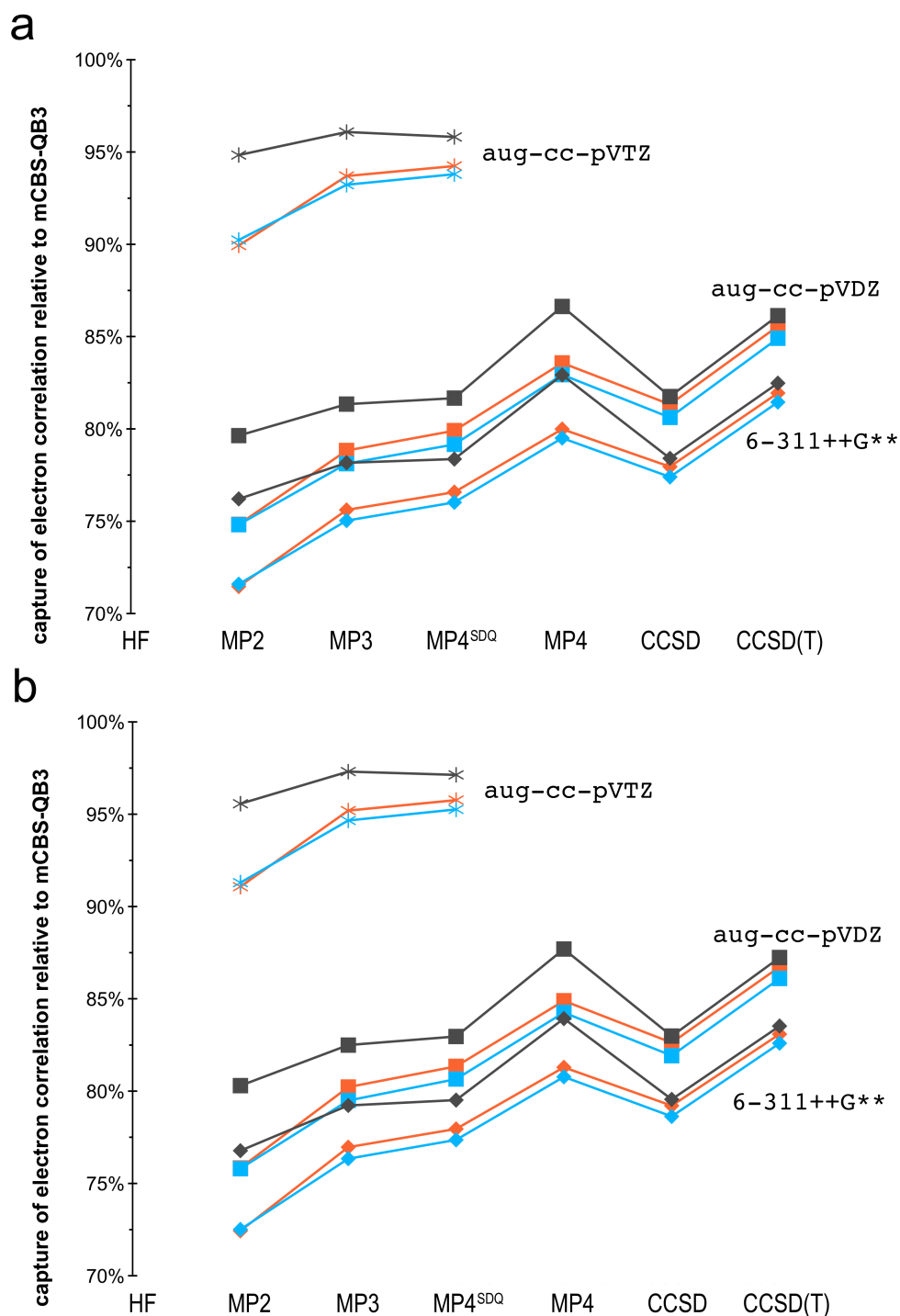


Figure S6. Comparison of the completeness of capturing electron correlation with the employed levels of correlated MO theory as a function of 6-311++G** (diamond), *aug-cc-pVDZ* (square), and *aug-cc-pVTZ* (star) basis sets for MPh (gray), B-MPh (orange) and N-MPh (light blue), for (a) the adsorbent models and (b) the adsorption models. The $1.2 \pm 0.2\%$ shift between the two sets of curves and the identical trends (parallel lines within 2% variation) between the results with and without the triples substitution (T) allows for the extrapolation of the missing CCSD and CCSD(T) results for the *aug-cc-pVTZ* basis set.

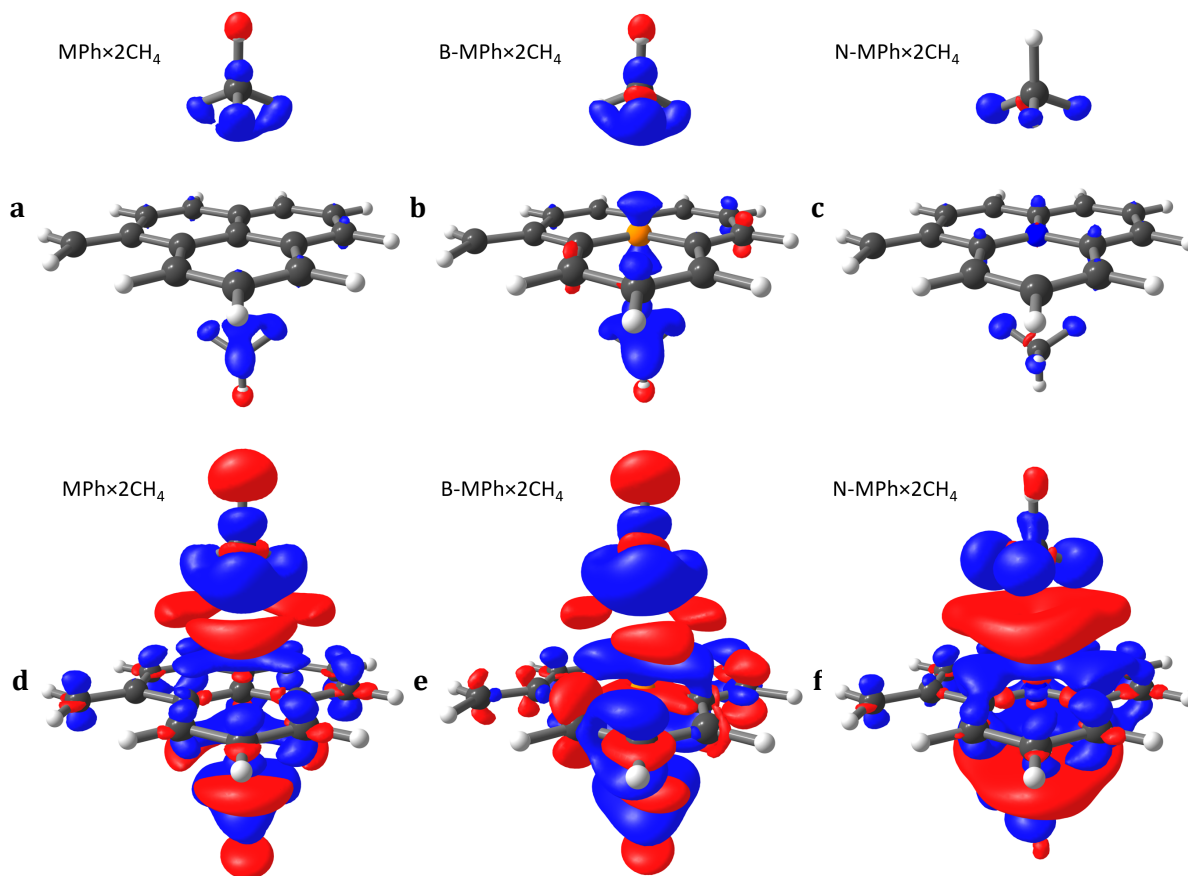


Figure S7. Electron density difference plots for methane interactions with MPh and its heteroatom-substituted variants: (a-c) at a high contour level of $5 \times 10^{-4} (e^-)^2 \text{ \AA}^{-3}$ and (d-f) at a low contour level of $1.5 \times 10^{-4} (e^-)^2 \text{ \AA}^{-3}$ for MPh \times 2CH $_4$ (a,d), B-MPh \times 2CH $_4$ (b,e), and N-MPh \times 2CH $_4$ (c,f). Electron density difference between the double adsorption model and the separate adsorbent and adsorbates at the MN15/def2-QZVPP level is shown (positive difference in red, negative difference in blue). See **Figure 3** for the corresponding single ($n = 1$) adsorption models.

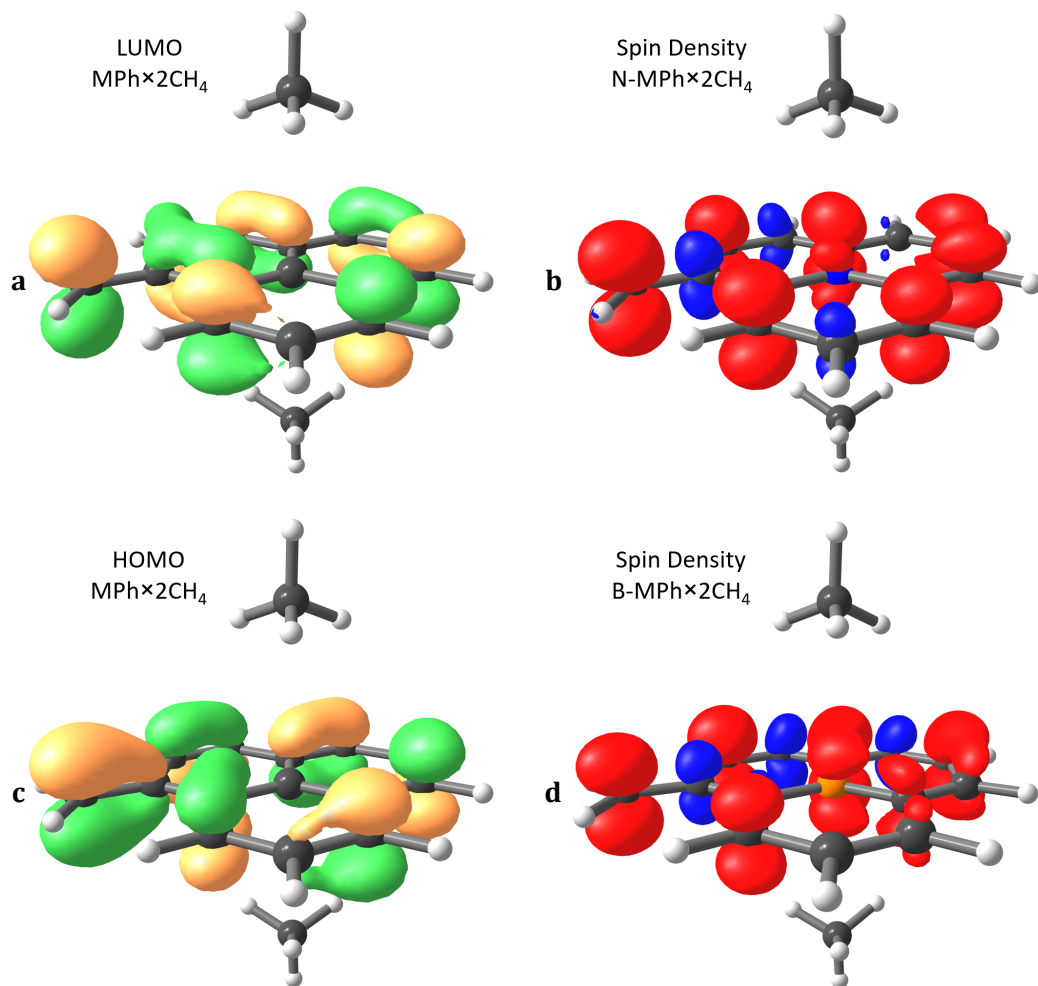


Figure S8. Comparison of the electron density of MPh and the spin density of B-MPh and N-MPh upon methane adsorption. (a) LUMO and (c) HOMO electron density contour plots for MPh×2CH₄ at a contour level of $4.5 \times 10^{-2} (e^-)^2 \text{ \AA}^{-3}$ and (b,d) spin density contour plots for N-MPh×2CH₄ and B-MPh×2CH₄ at a contour level of $3.5 \times 10^{-3} (e^-)^2 \text{ \AA}^{-3}$. See **Figure 4** for the corresponding single ($n = 1$) adsorption models.

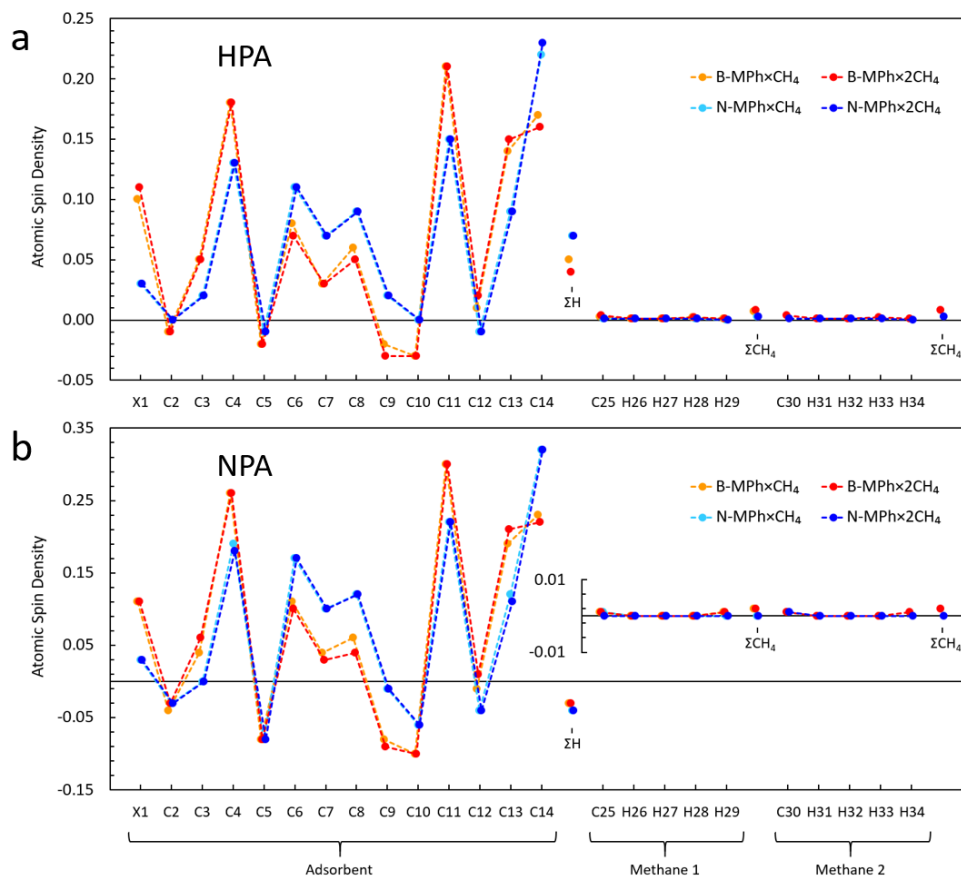


Figure S9. Atomic spin density distribution analysis upon single ($n = 1$) and double ($n = 2$) methane adsorption on B-MPh (orange/red) and N-MPh (cyan/blue) determined by two conceptually different population analysis methods: (a) Hirshfeld (HPA) and (b) Weinhold (NPA), at the MN15/def2-QZVPP level of theory. See **Figures S1-S3** for the atomic numbering and **Tables S11-S12** for the tabulated data.

The unpaired electron distribution among the atomic constituents of the $MPh \times nCH_4$ adsorption models at the MN15+ level, as calculated by the HPA and NPA analysis methods, is shown in **Figure S8** (see also **Tables S9-S10**). Contrary to the variations in atomic charges that are the sum of spin-up (α) and spin-down (β) one-electron densities (wherein errors accumulate), the spin densities show only negligible dependence on the population analysis method (due to error cancelation). The Weinhold analysis (NPA) displays a slightly larger spin polarization than the Hirshfeld analysis (HPA); however, the overall spin density distribution as a function of atom location in the adsorption system is identical in both cases. The different compositions of the spin-up and spin-down orbitals, and thus the multi-reference nature of the wave function, are demonstrated by the presence of both positively and negatively signed atomic spin densities in an ordered and characteristic manner, independent of the identity of substitution. While the atomic charge distribution undulates (**Figure 2** and **Tables S9-S10**) as a function of distance from the site of substitution (X1), the atomic spin densities show the opposite trend as the peripheral (γ) atoms accumulate the largest spin density. Exploratory calculations using larger, extended *maquette*

molecules (results not shown) confirm that the extra electron/electron hole delocalizes to the periphery of the conjugated polycyclic molecule and does not stay localized to the inner or outer sphere of the site of substitution as the origin of spin polarization. Hirshfeld analysis (HPA) shows to a greater extent than Weinhold analysis (NPA) that the methane adsorbate also undergoes a slight spin polarization: 0.008 e⁻ for B-MPh×nCH₄ and 0.003 e⁻ N-MPh×nCH₄ (**Figure 5** and **Table S12**). This is a direct indication of the presence of a small, but non-negligible magnetic interaction between the adsorbate and adsorbent in addition to the above discussed induced ionic interactions due to mutual polarization of the constituents of the adsorption system.

To a modest degree, the spin polarization also appears in the expectation value of the spin operator $\langle S^2 \rangle$ at the MN15+ level. The $\langle S^2 \rangle$ values are 0.791 and 0.783 for B-MPh×nCH₄ and N-MPh×nCH₄, respectively. Upon spin annihilation by eliminating contributions from the $M_s = \frac{1}{2}$ sublevel of the higher $S = \frac{3}{2}$ spin state, the $\langle S^2 \rangle$ values for both systems are reduced to 0.751, which is close to the ideal, non-contaminated expectation value of $S(S+1) = 0.750$. The reference wave function level for correlated MO calculations (HF/6-311++G**) shows a dramatically larger deviation from the ideal value (2.486 and 2.448). This result becomes even greater (4.982 and 4.725) upon spin annihilation, indicating significant contributions of the $M_s = \frac{1}{2}$ sublevel of the $S = \frac{5}{2}$ and likely higher spin states. Deviations from the ideal spin expectation value can be mitigated by constructing a restricted open-shell (ROHF) $S = \frac{1}{2}$ electronic structure calculation; however, this wave function corresponds to a significantly higher energy state by +173 and +158 kJ mol⁻¹ for the B-MPh×CH₄ and N-MPh×CH₄ models, respectively. These large energy values are indicative of the significant static electron correlation as captured by allowing for different composition of spin-up and spin-down one-electron orbitals in the unrestricted (UHF) calculation. Analogously, the use of the spin-polarized B-MPh×CH₄ and N-MPh×CH₄ electronic structures as initial wave functions results in a spin-unrestricted, open-shell singlet electronic structure for the unsubstituted MPh×CH₄ *maquette* at a lower energy structure (-110 kJ mol⁻¹) than the closed-shell, diamagnetic state, at the restricted HF/6-311++G** level. The energy differences between the spin-polarized (UHF) and spin-restricted (ROHF) electronic structures are gradually diminished as more complete treatment of electron correlation is employed: 264-287 at MP2, 138-152 at MP3, 98-112 at MP4^{SDQ}, 19-30 at CCSD, and finally 43-47 at CCSD(T), in kJ mol⁻¹. The complexity of the spin manifold also explains the computational challenges of obtaining equilibrium structures that were burdened by chronic oscillations in SCF cycles, jumping arbitrarily to higher energy potential energy surfaces that correspond to resonance structures with non-planar, puckered geometries. Further multi-reference CASSCF/CASMP2 calculations are warranted in order to obtain a complete, detailed picture of methane interactions with MPh-based molecular *maquettes* of carbon surfaces, but remain relegated to future work.

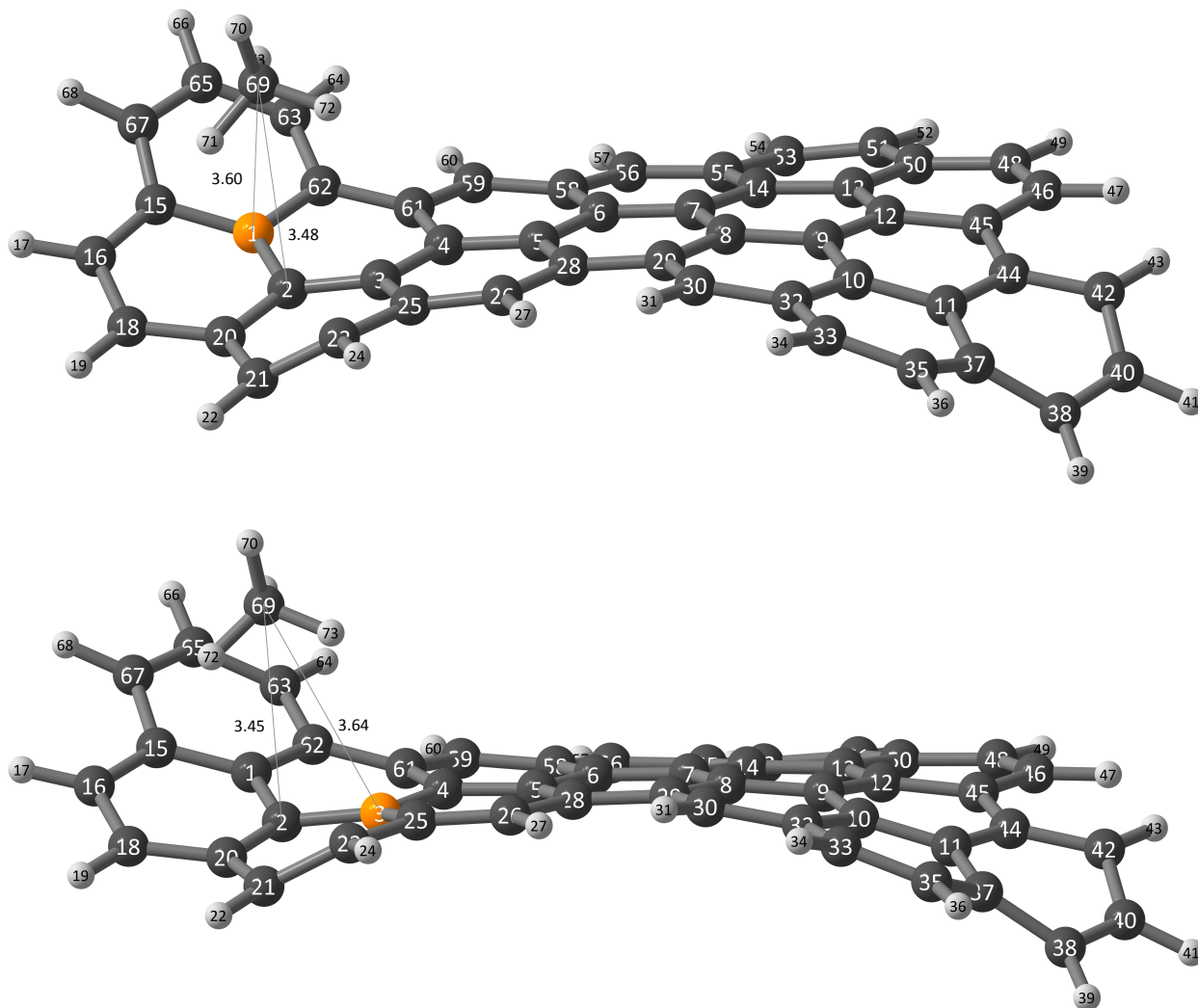


Figure S10. Stationary structures of the two “curved blade” adsorption models (BC₄₇H₂₀), where the CH₄ adsorbate slipped to an adjacent adsorption site due to the curvature and distortion of the aromatic π -system. Optimization was performed at the MN15/6-31G* (MN15-) level.

Table S1: Overview of literature examples of experimental (top) and theoretical (bottom) investigations of methane adsorption on carbon surfaces. The sign convention corresponds to energy of dissociation/desorption. All experimental and theoretical values refer to isosteric heat of desorption (q_{st}) from gas adsorption measurements and calculated desorption energy ($\Delta_{des}E$) from quantum potential energy differences, respectively.

Experimental Studies:

Author(s)	Year	DOI	Adsorbent		Method	q_{st} , kJ mol ⁻¹
Chahine	1997	10.1021/la960843x	activated carbon		Gas adsorption	
Salem	1998	10.1021/la970119u	activated carbon		Gas adsorption	14.35
Lozano-Castelló	2002	10.1016/S0008-6223(02)00194-X	activated carbon		Gas adsorption	
Zhou	2007	10.1021/jp074889i	MOFs		Gas adsorption	~12.2
Stadie	2013	10.1021/ja311415m	microporous carbons		Gas adsorption	13.5...19.5
Yuan	2013	10.1021/es4000643	ordered mesoporous carbon		Gas adsorption	15.4
Stadie	2015	10.1021/acs.jpcc.5b05021	microporous carbons		Gas adsorption	~14, 15, 19
Kim	2018	10.1016/j.micromeso.2018.06.021	N-doped nitrogen-doped crab shell-derived carbon nanofibers		Gas adsorption	18.9...20.7

Theoretical Studies:

Author(s)	Year	DOI	Adsorbent		Theory	$\Delta_{des}E$, kJ mol ⁻¹
Matranga	1992	10.1016/0009-2509(92)85005-V	activated carbon		GCMC, isosteric	~12 ^a
Cracknell	1993	10.1021/j100104a036	microporous carbon		GCMC, isosteric	~12 ^a
Bhatia	2006	10.1021/la0523816	porous carbon		GCMC, isosteric	16
Palmer	2009	10.1016/j.carbon.2009.06.037	coal-based activated carbon		GCMC, isosteric	~19 ^a
Smith	2012	10.1021/ct3008809	polyaromatic hydrocarbons		CCSD(T)+MP2	~14...~20
Lui	2013	10.1016/j.apsusc.2013.08.035	graphene		DFT (LDA CA-PZ)	9.8...14.9
Chen	2015	10.1109/LED.2015.2492580	monolayer and multilayer graphene		DFT (LDA GGA)	43.4
Hussain	2015	10.1002/jcc.24242	buckybowls		DFT (M05-2X)	4.6...20.3
Burrill	2020	10.1039/D0CP02645J	coronene		DFT (M05-2X)	4.6...20.3
			buckybowls		DFT (ω B97M-V/pc-2)	7.23...23.3
Denis	2008	10.1016/j.chemphys.2008.07.024	N-doped nanotube segments		DFT (LDA)	10.3...31.0
Lui	2013	10.1016/j.apsusc.2013.08.035	B-doped graphene		DFT (LDA CA-PZ)	6.2...14.8
			N-doped graphene		DFT (LDA CA-PZ)	2.9...17.3
Wang	2015	10.1002/pssb.201451632	N-doped graphene		DFT (PBE)	10.6...206.5
Chen	2015	10.1109/LED.2015.2492580	B-doped monolayer and multilayer graphene		DFT (LDA GGA)	49.2
			N-doped monolayer and multilayer graphene		DFT (LDA GGA)	41.5
Hassani	2016	10.1016/j.comptc.2016.02.019	B-doped graphene		DFT D3	7.5...17.5
			N-doped graphene		DFT D3	5.4...13.4

^a isosteric heat value.

Table S2. Graphical illustration and Z-matrix definitions for κ^1 , μ_2 , μ_3 , and η^2 approaches of CH₄ to the X1 position of MPh and its heteroatom substituted variants.

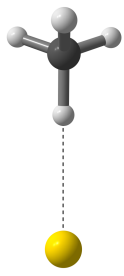
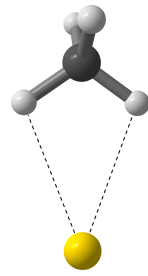
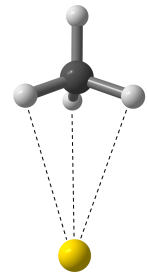
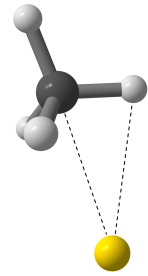
κ^1 CH ₄ bonding	μ_2 CH ₄ bonding	μ_3 CH ₄ /tetrel bonding	η^2 (C-H) CH ₄ bonding
			
B/C/N H 1 rCH X 2 1.0 190.0 C 2 rCHm 3 qCHX 1 wCHXC H 4 rCHm 2 qHCH 3 -wHaCHX H 4 rCHm 2 qHCH 3 wHbCHX H 4 rCHm 2 qHCH 3 wHaCHX C 1 rCaC 2 qCaCH 3 wCaaCHX C 1 rCaC 2 qCaCH 3 wCabCHX C 1 rCaC 2 qCaCX 3 -wCaaCXX C 8 rCbCa 1 qCbCaC 2 -wCbCaCH C 8 rCbCa 1 qCbCaC 2 wCbCaCH C 9 rCbCa 1 qCbCaC 2 wCbCaCH C 9 rCbCa 1 qCbCaC 2 -wCbCaCH C 10 rCbCa 1 qCbCaC 2 -wCbCaCH C 10 rCbCa 1 qCbCaC 2 -wCbCaCH C 10 rCbCa 1 qCbCaC 2 -wCbCaCH C 11 rCmCb 8 qCmCbCa 1 wCmCbCaC H 17 rHCm 11 qHCmCb 8 wHCmCbH H 17 rHCm 11 qHCmCb 8 wHCmCbH C 11 rCcCb 8 qCcCbCa 1 wCcCbCaC H 20 rHC 11 qHCcCb 8 wHCcCbCa C 12 rCcCb 8 qCcCbCa 1 wCcCbCaC H 22 rHC 11 qHCcCb 8 wHCcCbCa C 14 rCcCb 9 qCcCbCa 1 wCcCbCaC H 24 rHC 14 qHCcCb 9 wHCcCbCa H 12 rHC 8 qHCbCa 1 qHCbCaC H 13 rHC 9 qHCbCa 1 qHCbCaC H 14 rHC 9 qHCbCa 1 qHCbCaC H 15 rHC 10 qHCbCa 1 qHCbCaC H 16 rHC 10 qHCbCa 1 qHCbCaC rCH 3.0 8 -0.25 rCHm 1.09 qCHX 88.9 8 -11.1 wCHXC 180.0 qHCH 120.0 wHaCHX 60.0 wHbCHX 180.0 rCaC 1.435 qCaCH 90.0 wCaaCHX 180.0 wCabCHX 60.0 rCbCa 1.435 qCbCaC 120.0 wCbCaCH 90.0 rCmCb 1.36 qCmCbCa 120.0 wCmCbCaC 180.0 rHCm 1.1 qHCmCb 120.0 wHCmCbCa 0.0 wHCmCbH 180.0 rCcCb 1.4 qCcCbCa 120.0 wCcCbCaC 0.0 rHC 1.09 qHCcCb 120.0 wHCcCbCa 180.0 qHCbCa 120.0 qHCbCaC 180.0	B/C/N X 1 rCX X 2 rXX 1 qXXC C 2 rCX 3 qCXX 1 wCXXC H 4 rHC 3 qHCX 1 wHCXC H 4 rHC 5 qHCH 1 wHaCHC H 4 rHC 5 qHCH 1 -wHbCHC H 4 rHC 5 qHCH 1 wHcCHC C 1 rCaC 2 qCaCX 3 wCaaCXX C 1 rCaC 2 qCaCX 3 -wCaaCXX C 1 rCaC 2 qCaCX 3 wCabCXX C 9 rCbCa 1 qCbCaC 2 -wCbCaCX C 9 rCbCa 1 qCbCaC 2 wCbCaCX C 10 rCbCa 1 qCbCaC 2 wCbCaCX C 10 rCbCa 1 qCbCaC 2 -wCbCaCX C 11 rCbCa 1 qCbCaC 2 -wCbCaCX C 11 rCbCa 1 qCbCaC 2 wCbCaCX C 12 rCmCb 9 qCmCbCa 1 wCmCbCaC H 18 rHCm 12 qHCmCb 9 wHCmCbCa H 18 rHCm 12 qHCmCb 9 wHCmCbH C 12 rCcCb 9 qCcCbCa 1 wCcCbCaC H 21 rHCc 12 qHCcCb 9 wHCcCbCa C 13 rCcCb 9 qCcCbCa 1 wCcCbCaC H 23 rHCc 13 qHCcCb 9 wHCcCbCa C 15 rCcCb 10 qCcCbCa 1 wCcCbCaC H 25 rHCc 15 qHCcCb 10 wHCcCbCa H 13 rHCb 9 qHCbCa 1 wHCbCaC H 14 rHCb 10 qHCbCa 1 wHCbCaC H 15 rHCb 10 qHCbCa 1 wHCbCaC H 16 rHCb 11 qHCbCa 1 wHCbCaC H 17 rHCb 11 qHCbCa 1 wHCbCaC	B/C/N X 1 rCX X 2 rXX 1 qXXC C 2 rCX 3 qCXX 1 wCXXC H 4 rHC 2 qHCX 3 wHCXC H 4 rHC 5 qHCH 3 wHaCHX H 4 rHC 5 qHCH 3 wHbCHX H 4 rHC 5 qHCH 3 -wHbCHX C 1 rCaC 2 qCaCX 3 wCaaCXX C 1 rCaC 2 qCaCX 3 -wCaaCXX C 1 rCaC 2 qCaCX 3 wCabCXX C 9 rCbCa 1 qCbCaC 2 -wCbCaCX C 9 rCbCa 1 qCbCaC 2 wCbCaCX C 10 rCbCa 1 qCbCaC 2 wCbCaCX C 10 rCbCa 1 qCbCaC 2 -wCbCaCX C 11 rCbCa 1 qCbCaC 2 -wCbCaCX C 11 rCbCa 1 qCbCaC 2 wCbCaCX C 12 rCmCb 9 qCmCbCa 1 wCmCbCaC H 18 rHCm 12 qHCmCb 9 wHCmCbCa H 18 rHCm 12 qHCmCb 9 wHCmCbH C 12 rCcCb 9 qCcCbCa 1 wCcCbCaC H 21 rHCc 12 qHCcCb 9 wHCcCbCa C 13 rCcCb 9 qCcCbCa 1 wCcCbCaC H 23 rHCc 13 qHCcCb 9 wHCcCbCa C 15 rCcCb 10 qCcCbCa 1 wCcCbCaC H 25 rHCc 15 qHCcCb 10 wHCcCbCa H 13 rHCb 9 qHCbCa 1 wHCbCaC H 14 rHCb 10 qHCbCa 1 wHCbCaC H 15 rHCb 10 qHCbCa 1 wHCbCaC H 16 rHCb 11 qHCbCa 1 wHCbCaC H 17 rHCb 11 qHCbCa 1 wHCbCaC	B/C/N C X 1 rCX H 2 rHX 1 qHXC C 3 rCH 2 qCHX 1 wCHXC H 4 rHC 3 qHCH 1 -wHaCHC H 4 rHC 3 qHCH 1 wHbCHC H 4 rHC 3 qHCH 1 wHaCHC C 1 rCaC 2 qCaCX 4 wCaaCXXC C 1 rCaC 2 qCaCX 4 -wCabCXXC C 1 rCaC 2 qCaCX 4 wCabCXXC C 8 rCbCa 1 qCbCaC 2 -wCbCaCX C 8 rCbCa 1 qCbCaC 2 wCbCaCX C 9 rCbCa 1 qCbCaC 2 wCbCaCX C 9 rCbCa 1 qCbCaC 2 -wCbCaCX C 10 rCbCa 1 qCbCaC 2 wCbCaCX C 10 rCbCa 1 qCbCaC 2 -wCbCaCX C 11 rCmCb 8 qCmCbCa 1 wCmCbCaC H 17 rHCm 11 qHCmCb 8 wHCmCbH H 17 rHCm 11 qHCmCb 8 wHCmCbH C 11 rCcCb 8 qCcCbCa 1 wCcCbCaC H 20 rHC 11 qHCcCb 8 wHCcCbCa C 12 rCcCb 8 qCcCbCa 1 wCcCbCaC H 22 rHC 11 qHCcCb 8 wHCcCbCa C 14 rCcCb 9 qCcCbCa 1 wCcCbCaC H 24 rHC 14 qHCcCb 9 wHCcCbCa H 12 rHC 8 qHCbCa 1 qHCbCaC H 13 rHC 9 qHCbCa 1 qHCbCaC H 14 rHC 9 qHCbCa 1 qHCbCaC H 15 rHC 10 qHCbCa 1 qHCbCaC H 16 rHC 10 qHCbCa 1 qHCbCaC

Table S3. Free adsorbent structures (LoT: MN15 using the STO-3G {MN15}, SDDAll [MN15], 6-31G* (MN15-),def2-QZVPP (MN15+), or *aug-cc-pVTZ* (MN15cc) basis sets) of MPh, B-MPh, and N-MPh as described by averages and standard deviations of inner, outer, and peripheral sphere C–C distances in Å, out-of-planarity (δ , in Å) of the site of substitution, and wagging angle (w , in degrees) of the methyldene group (see **Table S4** for the geometry upon methane adsorption).

Adsorbent	LoT	Inner, Å	Outer, Å	Peripheral, Å	δ , Å	w , °
MPh	{MN15}	1.44±0.01	1.43±0.05	1.41±0.05	0.00	177
	[MN15]	1.43±0.00	1.42±0.04	1.40±0.04	0.00	177
	MN15-	1.43±0.00	1.42±0.04	1.40±0.04	0.00	176
	MN15+	1.42±0.00	1.41±0.04	1.39±0.04	0.00	176
	MN15cc	1.42±0.00	1.41±0.04	1.39±0.04	0.00	176
B-MPh	{MN15}	1.52±0.01	1.44±0.05	1.42±0.05	0.00	174
	[MN15]	1.52±0.01	1.42±0.04	1.41±0.04	0.00	173
	MN15-	1.52±0.01	1.42±0.04	1.41±0.04	0.00	172
	MN15+	1.51±0.01	1.41±0.04	1.41±0.04	0.00	172
	MN15cc	1.51±0.01	1.41±0.04	1.41±0.04	0.00	172
N-MPh	{MN15}	1.44±0.01	1.44±0.05	1.41±0.04	0.00	179
	[MN15]	1.41±0.01	1.42±0.04	1.39±0.03	0.00	179
	MN15-	1.41±0.01	1.42±0.04	1.39±0.03	0.01	179
	MN15+	1.40±0.01	1.41±0.04	1.39±0.03	0.00	179
	MN15cc	1.40±0.01	1.41±0.04	1.39±0.03	0.00	179

Table S4. Adsorbent structures upon adsorption (LoT: MN15, MP2, MP4^{SDQ}, or CCSD using the 6-311++G** basis set, or MN15 using the STO-3G {MN15}, SDDAll [MN15], 6-31G* (MN15-), def2-QZVPP (MN15+), or *aug-cc-pVTZ* (MN15cc) basis sets) of methane on MPh, B-MPh, and N-MPh, as described by averages and standard deviations of inner, outer, and peripheral sphere C-C distances in Å, out-of-planarity (δ , in Å) of the site of substitution, and wagging angle (w , in degrees) of the methyldene group (see **Tables 1** and **S3** for the free adsorbent structures).

Adsorbent	LoT	n	Inner, Å	Outer, Å	Peripheral, Å	δ , Å	w , °	
MPh	{MN15}	1	1.44±0.01	1.43±0.05	1.41±0.05	0.01	177	
	[MN15]	1	1.43±0.00	1.42±0.04	1.40±0.04	0.03	176	
	MN15-	1	1.43±0.00	1.42±0.04	1.40±0.04	0.03	175	
	MN15	1	1.43±0.00	1.42±0.04	1.40±0.04	0.03	175	
	MN15+	1	1.42±0.00	1.41±0.04	1.39±0.04	0.03	176	
	MN15cc	1	1.42±0.00	1.41±0.04	1.39±0.04	0.03	176	
	MP2	1	1.54±0.00	1.40±0.05	1.41±0.05	0.03	171	
	MP4 ^{SDQ}	1	1.43±0.01	1.42±0.04	1.40±0.04	0.05	173	
	CCSD	1	1.43±0.01	1.42±0.04	1.40±0.04	0.04	173	
	{MN15}	2	1.44±0.01	1.43±0.05	1.41±0.05	0.00	177	
	[MN15]	2	1.43±0.00	1.42±0.04	1.40±0.04	0.00	177	
	MN15-	2	1.43±0.00	1.42±0.04	1.40±0.04	0.00	176	
	MN15	2	1.43±0.00	1.42±0.04	1.39±0.04	0.00	176	
	MN15+	2	1.42±0.00	1.41±0.04	1.39±0.04	0.00	176	
	MN15cc	2	1.42±0.00	1.41±0.04	1.39±0.04	0.00	176	
	B-MPh	{MN15}	1	1.52±0.01	1.44±0.05	1.43±0.05	0.00	174
		[MN15]	1	1.52±0.01	1.42±0.04	1.41±0.04	0.02	173
		MN15-	1	1.52±0.01	1.42±0.04	1.41±0.04	0.04	172
MN15		1	1.52±0.01	1.42±0.04	1.41±0.04	0.04	172	
MN15+		1	1.52±0.01	1.41±0.04	1.41±0.04	0.04	172	
MN15cc		1	1.52±0.01	1.41±0.04	1.41±0.04	0.04	172	
MP2		1	1.54±0.00	1.40±0.05	1.41±0.05	0.03	171	
MP4 ^{SDQ}		1	1.54±0.00	1.41±0.04	1.42±0.04	0.02	173	
CCSD		1	1.54±0.01	1.42±0.05	1.42±0.05	0.04	171	
{MN15}		2	1.52±0.01	1.43±0.05	1.43±0.05	0.00	174	
[MN15]		2	1.52±0.01	1.42±0.04	1.41±0.04	0.00	173	
MN15-		2	1.52±0.01	1.42±0.04	1.41±0.04	0.00	172	
MN15		2	1.52±0.01	1.42±0.04	1.41±0.04	0.00	172	
MN15+		2	1.52±0.01	1.41±0.04	1.41±0.04	0.00	172	
MN15cc		2	1.52±0.01	1.41±0.04	1.41±0.04	0.00	172	

Table S4. continued

N-MPh	{MN15}	1	1.44±0.01	1.44±0.05	1.41±0.04	0.01	179
	[MN15]	1	1.41±0.01	1.42±0.04	1.39±0.03	0.03	178
	MN15-	1	1.41±0.01	1.42±0.04	1.39±0.03	0.03	175
	MN15	1	1.41±0.01	1.42±0.04	1.39±0.03	0.02	177
	MN15+	1	1.40±0.01	1.41±0.04	1.39±0.03	0.02	178
	MN15cc	1	1.40±0.01	1.41±0.04	1.39±0.03	0.02	178
	MP2	1	1.41±0.01	1.41±0.01	1.39±0.03	0.01	175
	MP4 ^{SDQ}	1	1.41±0.01	1.42±0.02	1.39±0.03	0.01	176
	CCSD	1	1.42±0.01	1.42±0.07	1.41±0.05	0.07	169
	{MN15}	2	1.44±0.0	1.44±0.05	1.41±0.04	0.00	179
	[MN15]	2	1.41±0.0	1.42±0.04	1.39±0.03	0.00	179
	MN15-	2	1.41±0.01	1.42±0.04	1.39±0.03	0.00	179
	MN15	2	1.41±0.01	1.42±0.04	1.39±0.03	0.00	179
	MN15+	2	1.40±0.01	1.41±0.04	1.39±0.03	0.00	179
	MN15cc	2	1.40±0.01	1.41±0.04	1.39±0.03	0.00	179

Table S5. Adsorption model structures (LoT: MN15 using the STO-3G {MN15}, SDDAll [MN15], 6-31G* (MN15-), or def2-QZVPP (MN15+), or *aug-cc-pVTZ* (MN15cc) basis sets) of methane on MPh, B-MPh, and N-MPh. Adsorption by one ($n = 1$) and two ($n = 2$) methane molecules is described by interaction distances and twisting angles: methane to central site (C25...X1) distance, proximal H to closest ring centroid ($H_p \cdots X_i$) distance, dihedral angle formed by $X_i \cdots X1 \cdots C25-H_p$ (ω), and proximal and distal C-H bond lengths.

Adsorbent	LoT	n	C25...X1, Å	$H_p \cdots X_i$, Å	ω , °	C-H _p , ^a Å	C-H _d , ^a Å
MPh	{MN15}	1	3.44	3.09±0.20	2±1	1.096±0.000	1.096
	[MN15]	1	3.29	2.92±0.03	0±1	1.091±0.000	1.090
	MN15-	1	3.28	2.90±0.04	1±1	1.094±0.000	1.093
	MN15+	1	3.28	2.91±0.04	0±0	1.089±0.000	1.087
	MN15cc	1	3.28	2.91±0.04	0±0	1.089±0.000	1.087
	{MN15}	2	3.56±0.01	3.23±0.38	10±4	1.096±0.000	1.096±0.000
	[MN15]	2	3.29±0.00	2.95±0.02	1±0	1.091±0.000	1.090±0.000
	MN15-	2	3.27±0.00	2.93±0.03	1±1	1.094±0.000	1.093±0.000
	MN15+	2	3.27±0.00	2.93±0.03	1±0	1.089±0.000	1.087±0.000
	MN15cc	2	3.27±0.00	2.93±0.03	1±0	1.089±0.000	1.087±0.000
B-MPh	{MN15}	1	3.45	3.11±0.28	2±1	1.096±0.000	1.096
	[MN15]	1	3.28	2.91±0.04	4±1	1.091±0.000	1.090
	MN15-	1	3.29	2.91±0.05	3±1	1.094±0.000	1.093
	MN15+	1	3.30	2.93±0.05	5±1	1.088±0.000	1.087
	MN15cc	1	3.30	2.93±0.05	5±1	1.088±0.000	1.087
	{MN15}	2	3.44±0.01	3.10±0.23	6±2	1.096±0.000	1.096±0.000
	[MN15]	2	3.26±0.00	2.92±0.04	4±1	1.091±0.000	1.090±0.000
	MN15-	2	3.27±0.00	2.93±0.05	2±1	1.094±0.000	1.093±0.000
	MN15+	2	3.29±0.00	2.95±0.04	4 ±1	1.088±0.000	1.087±0.000
	MN15cc	2	3.29±0.00	2.95±0.04	4 ±1	1.088±0.000	1.087±0.000
N-MPh	{MN15}	1	3.28	2.93±0.01	0±0	1.096±0.000	1.096
	[MN15]	1	3.17	2.82±0.01	7±11	1.091±0.000	1.089
	MN15-	1	3.17	2.80±0.01	1±1	1.095±0.000	1.093
	MN15+	1	3.17	2.81±0.00	1±1	1.089±0.000	1.087
	MN15cc						
	{MN15}	2	3.28±0.00	2.94±0.01	1±0	1.096±0.000	1.096±0.000
	[MN15]	2	3.17±0.00	2.83±0.01	1±1	1.091±0.000	1.089±0.000
	MN15-	2	3.16±0	2.82±0.01	1±1	1.095±0.000	1.093±0.000
	MN15+	2	3.16±0.00	2.82±0.01	1±1	1.089±0.000	1.087±0.000
	MN15cc	2	3.16±0.00	2.82±0.01	1±1	1.089±0.000	1.087±0.000

^aThe C-H bond lengths in free methane are, at {MN15}: 1.095 Å, [MN15]: 1.089 Å, MN15-: 1.092 Å; MN15+: 1.086 Å; and MN15cc: 1.087 Å

Table S6. Desorption energies (Δ_{des} , kJ mol⁻¹) for MPh×nCH₄ → MPh + nCH₄ (LoT: MN15 using the STO-3G {MN15}, SDDAll [MN15], 6-31G* (MN15-), def2-QZVPP (MN15+), or *aug-cc-pVTZ* (MN15cc) basis sets). mCBS-QB3 refers to the modified complete basis set extrapolation method employing the CBS-QB3 formalism, but utilizing the MN15/6-311++G** geometry (see Table S6.5 for details). The standard enthalpy, Gibbs free energy, and entropy of desorption are calculated at 298 K using a simple statistical mechanical model assuming ideal gas behavior. A modest statistical analysis (average and standard deviation) of the thermochemical quantities is shown, normalized per mole of CH₄.

Adsorbent	n	$\Delta_{\text{des}}U^{\text{QM}}$ (kJ mol ⁻¹)						BSSE (kJ mol ⁻¹)				
		{MN15}	[MN15]	MN15-	MN15+	MN15cc	mCBS-QB3	{MN15}	[MN15]	MN15-	MN15+	MN15cc
MPh	1	3	16	13	14	15	10	2.5	2.8	3.7	0.3	1.5
B-MPh	1	2	13	14	13	15	9	1.9	2.2	4.4	0.2	1.7
N-MPh	1	3	17	16	16	18	12	2.3	2.6	3.9	0.3	1.8
MPh	2	5	33	26	27	31	21	5.0	5.7	7.2	0.6	3.7
B-MPh	2	4	25	26	26	29	18	4.2	4.3	8.3	0.5	4.1
N-MPh	2	5	33	32	32	36	24	4.6	5.1	7.4	0.6	4.1
MPh	per CH ₄	2.5±0.0	16.3±0.0	13.0±0.2	13.6±0.3	15.3±0.0	10.2±0.2					
B-MPh	per CH ₄	2.0±0.1	12.8±0.3	13.3±0.2	13.2±0.3	14.6±0.1	8.9±0.1					
N-MPh	per CH ₄	2.7±0.0	16.5±0.2	16.2±0.4	16.2±0.2	18.0±0.0	12.2±0.0					

Adsorbent	n	$\Delta_{\text{des}}H^{\circ}$ (kJ mol ⁻¹)						$\Delta_{\text{des}}G^{\circ}$ (kJ mol ⁻¹)					
		{MN15}	[MN15]	MN15-	MN15+	MN15cc	mCBS-QB3	{MN15}	[MN15]	MN15-	MN15+	MN15cc	mCBS-QB3
MPh	1	-3	11	8	9	11	9	-28	-23	-28	-26	-24	-19
B-MPh	1	-3	8	9	9	10	7	-31	-27	-26	-25	-23	-19
N-MPh	1	-3	12	9	11	13	9	-40	-26	-23	-25	-22	-12
MPh	2	-3	23	16	16	21	18	-62	-46	-54	-51	-48	-34
B-MPh	2	-6	15	17	17	20	14	-56	-53	-51	-50	-47	-35
N-MPh	2	-7	23	21	22	26	22	-80	-51	-53	-50	-46	-35
MPh	per CH ₄	-1.9±0.9	11.5±0.0	7.9±0.2	8.7±0.3	10.7±0.2	8.8±0.0	-29.3±2.3	-23.1±0.2	-27.3±0.6	-13.1±0.6	-23.8±0.1	-18.0±1.0
B-MPh	per CH ₄	-3.2±0.2	7.8±0.2	8.4±0.2	8.4±0.3	10.1±0.2	7.2±0.0	-29.8±2.2	-26.8±0.4	-26.0±0.4	-12.6±0.3	-23.4±0.2	-18.2±1.5
N-MPh	per CH ₄	-3.4±0.1	11.4±0.2	9.6±1.5	11.2±0.2	13.3±0.2	9.9±1.6	-40.0±0.1	-25.7±0.3	-24.9±2.3	-12.7±0.3	-22.6±0.3	-14.5±4.2

Table S7. Energy components of the modified CBS-QB3 method using fixed MN15/6-311++G** equilibrium structures for adsorbent, adsorbate, and adsorption models and corresponding vibrational analyses (invoking Gaussian keyword 'StartMP2' and using the results of the frequency calculation from the converged MN15 checkpoints).

CBS-QB3		MN15/6-311G(2d,d,p) w/5d&7f								
(StartMP2:MN15)	$E^{nuc,rep}$, a.u.	E^{SCF} , a.u.	$\langle S^2 \rangle$		E^{ZPE} , a.u.	Q , a.u.	H , a.u.	G , a.u.	S , cal/molK	
			before	after						
CH ₄	13.4425	-40.5337	0.00	0.00	-40.4891	-40.4862	-40.4853	-40.5064		44.5
B-MPh	754.5442	-526.3362	0.78	0.75	-526.1510	-526.1408	-526.1399	-526.1873		99.8
MPh	787.1806	-539.6350	0.00	0.00	-539.4457	-539.4360	-539.4351	-539.4813		97.3
N-MPh	812.5538	-556.2317	0.77	0.75	-556.0449	-556.0357	-556.0348	-556.0796		94.4
B-MPh×CH ₄	888.0026	-566.8668	0.78	0.75	-566.6356	-566.6213	-566.6204	-566.6779		121.1
MPh×CH ₄	923.5009	-580.1662	0.00	0.00	-579.9307	-579.9170	-579.9160	-579.9718		117.4
N-MPh×CH ₄	953.3618	-596.7628	0.77	0.75	-596.5296	-596.5156	-596.5146	-596.5721		120.9
B-MPh×2CH ₄	1027.9738	-607.3976	0.78	0.75	-607.1207	-607.1019	-607.1010	-607.1706		146.5
MPh×2CH ₄	1066.4851	-620.6976	0.00	0.00	-620.4162	-620.3982	-620.3972	-620.4650		142.6
N-MPh×2CH ₄	1101.6539	-637.2941	0.77	0.75	-637.0149	-636.9976	-636.9966	-637.0610		135.6

CBS-QB3		CCSD(T)/6-31+G(d') w/6d&7f								
(StartMP2:MN15)	E^{SCF} , a.u.	$\langle S^2 \rangle$		E^{MP2} , a.u.	E^{MP3} , a.u.	E^{MP4sdq} , a.u.	E^{CCSD} , a.u.	$E^{CCSD(T)}$, a.u.		
		before	after							
CH ₄	-40.1954	0.00	0.00	-40.3359	-40.3525	-40.3561	-40.3568		-40.3597	
B-MPh	-522.7987	2.48	4.93	-524.3961	-524.4858	-524.5127	-524.5466		-524.6339	
MPh	-535.9817	0.00	0.00	-537.7811	-537.8228	-537.8343	-537.8357		-537.9302	
N-MPh	-552.5321	2.44	4.70	-554.2292	-554.3089	-554.3377	-554.3735		-554.4669	
B-MPh×CH ₄	-562.9909	2.48	4.93	-564.7377	-564.8431	-564.8736	-564.9080		-564.9990	
MPh×CH ₄	-576.1732	0.00	0.00	-578.1241	-578.1802	-578.1953	-578.1973		-578.2960	
N-MPh×CH ₄	-592.7234	2.44	4.68	-594.5722	-594.6670	-594.6994	-594.7361		-594.8339	
B-MPh×2CH ₄	-603.1836	2.48	4.93	-605.0798	-605.2009	-605.2350	-605.2698		-605.3645	
MPh×2CH ₄	-616.3653	0.00	0.00	-618.4667	-618.5375	-618.5563	-618.5588		-618.6616	
N-MPh×2CH ₄	-632.9153	2.44	4.67	-634.9153	-635.0253	-635.0614	-635.0988		-635.2009	

CBS-QB3		MP4SDQ/CBSB4 w/6d&7f					MP2/CBSB3 w/5d&7f				
(StartMP2:MN15)	E^{SCF} , a.u.	$\langle S^2 \rangle$		E^{MP2} , a.u.	E^{MP3} , a.u.	E^{MP4sdq} , a.u.	E^{SCF} , a.u.	$\langle S^2 \rangle$		E^{MP2} , a.u.	
		before	after					before	after		
CH ₄	-40.2010	0.00	0.00	-40.3675	-40.3870	-40.3896	-40.2122	0.00	0.00	-40.4043	
B-MPh	-522.8146	2.47	4.91	-524.4734	-524.5691	-524.5934	-522.9430	2.47	4.89	-524.8981	
MPh	-535.9981	0.00	0.00	-537.8585	-537.9058	-537.9144	-536.1318	0.00	0.00	-538.3024	
N-MPh	-552.5487	2.44	4.68	-554.3070	-554.3924	-554.4187	-552.6910	2.43	4.63	-554.7694	
B-MPh×CH ₄	-563.0123	2.47	4.92	-564.8465	-564.9604	-564.9874	-563.1520	2.47	4.90	-565.3077	
MPh×CH ₄	-576.1952	0.00	0.00	-578.2331	-578.2974	-578.3087	-576.3402	0.00	0.00	-578.7136	
N-MPh×CH ₄	-592.7455	2.44	4.66	-594.6817	-594.7848	-594.8138	-592.8989	2.43	4.62	-595.1803	
B-MPh×2CH ₄	-603.2106	2.47	4.91	-605.2197	-605.3520	-605.3816	-603.3615	2.47	4.90	-605.7178	
MPh×2CH ₄	-616.3928	0.00	0.00	-618.6072	-618.6888	-618.7028	-616.5493	0.00	0.00	-619.1250	
N-MPh×2CH ₄	-632.9430	2.43	4.65	-635.0563	-635.1771	-635.2090	-633.1075	2.43	4.61	-635.5915	

Table S7. continued.

CBS-QB3 (StartMP2:MN15)	CBS-MN15 technical												
	EISum	E2(CBS)	CBS-Int	OTii	E(ZPE)	E(thermal)	E(SCF)	$\Delta E(MP2)$	$\Delta E(CBS)$	$\Delta E(MP34)$	$\Delta E(CCSD)$	$\Delta E(Int)$	$\Delta E(empirical)$
CH ₄	5.0	-0.2114	0.0073	2.0796	0.0442	0.0471	-40.2122	-0.1920	-0.0194	-0.0222	-0.0036	0.0073	-0.0120
B-MPh	93.0	-2.1436	0.0617	15.5321	0.1864	0.1968	-522.9431	-1.9550	-0.1886	-0.1200	-0.1212	0.0617	-0.1063
MPh	47.0	-2.3729	0.0698	16.2389	0.1906	0.2005	-536.1318	-2.1706	-0.2023	-0.0559	-0.0960	0.0698	-0.0940
N-MPh	95.0	-2.2800	0.0642	16.2173	0.1878	0.1972	-552.6910	-2.0784	-0.2016	-0.1117	-0.1293	0.0642	-0.1099
B-MPh×CH ₄	103.0	-2.3639	0.0691	17.5837	0.2319	0.2468	-563.1520	-2.1558	-0.2081	-0.1409	-0.1255	0.0691	-0.1182
MPh×CH ₄	52.0	-2.5952	0.0772	18.2867	0.2364	0.2505	-576.3402	-2.3734	-0.2218	-0.0756	-0.1007	0.0772	-0.1059
N-MPh×CH ₄	105.0	-2.5026	0.0717	18.2664	0.2337	0.2482	-592.8989	-2.2814	-0.2211	-0.1321	-0.1345	0.0717	-0.1218
B-MPh×2CH ₄	113.0	-2.5835	0.0764	19.6337	0.2774	0.2967	-603.3615	-2.3564	-0.2271	-0.1619	-0.1296	0.0764	-0.1301
MPh×2CH ₄	57.0	-2.8164	0.0845	20.3359	0.2819	0.3006	-616.5493	-2.5756	-0.2407	-0.0955	-0.1054	0.0845	-0.1177
N-MPh×2CH ₄	115.0	-2.7241	0.0789	20.3144	0.2794	0.2973	-633.1075	-2.4840	-0.2400	-0.1527	-0.1395	0.0789	-0.1336

CBS-QB3 (StartMP2:MN15)	CBS-MN15 (NoOpt) final at 298.15 K 1 atm (0 Kelvin) U, a.u. H, a.u. G, a.u.			
CH ₄	-40.4099	-40.4071	-40.4061	-40.4273
B-MPh	-525.1861	-525.1757	-525.1748	-525.2225
MPh	-538.4902	-538.4804	-538.4794	-538.5259
N-MPh	-555.0698	-555.0604	-555.0595	-555.1046
B-MPh×CH ₄	-565.5994	-565.5846	-565.5837	-565.6425
MPh×CH ₄	-578.9040	-578.8898	-578.8889	-578.9459
N-MPh×CH ₄	-595.4844	-595.4699	-595.4689	-595.5274
B-MPh×2CH ₄	-606.0128	-605.9935	-605.9925	-606.0637
MPh×2CH ₄	-619.3180	-619.2993	-619.2984	-619.3676
N-MPh×2CH ₄	-635.8990	-635.8811	-635.8802	-635.9458

Table S8. Energy stabilization ($\Delta\Delta E^{\text{QM}}$) and desorption ($\rightarrow\text{MPh}+\text{CH}_4$) energy differences (in kJ mol^{-1}) due to optimizing the MN16/6-311++G** equilibrium structures of the adsorbent, adsorbate, and the adsorption model using a conceptually converging series of correlated MO theories (LoT: MP2, MP3, MP4, CCSD, or CCSD(T) using the 6-311++G** basis set).

$\Delta\Delta E^{\text{QM}}$	MP2	MP3	MP4 ^a	CCSD	CCSD(T) ^b
MPh	-10	-5	-10	-6	-9
B-MPh	-10	-8	-9	-7	-7
N-MPh	-13	-9	-15	-11	-10
CH ₄	< 0.1	< 0.1	< 0.1	< 0.1	< 0.1
MPh×CH ₄	-9	-5	-8	-5	-8
B-MPh×CH ₄	-9	-8	-9	-7	-6
N-MPh×CH ₄	-10	-10	-9	-8	-12
$\rightarrow\text{MPh}+\text{CH}_4$	-1	0	-2	-1	-1
$\rightarrow\text{B-MPh}+\text{CH}_4$	-1	0	0	0	-1
$\rightarrow\text{N-MPh}+\text{CH}_4$	-3	+2	-6	-3	+2

^aMP4 results are single-point energy calculations using the MP4^{SDQ} geometry (i.e., MP4|MP4^{SDQ}).

^bCCSD(T) results are single-point energy calculations using the CCSD geometry (i.e., CCSD(T)|CCSD)

Table S9. Atomic charge (electron) distribution analysis upon single (n = 1) and double (n = 2) methane adsorption on MPh, B-MPh, and N-MPh determined by three conceptually different population analysis methods: Hirshfeld (HPA), Weinhold (NPA), and Merz-Kollman (ESP) at the MN15/def2-QZVPP level of theory. See **Figure 2** for a graphical plot and **Figure S1** for the numbering of atom positions.

X	n	X1	C2	α C3	C4	C5	C6	β C7	C8	C9	C10	C11	γ C12	C13	=CH ₂ C14	Σ H
Hirshfeld Population Analysis (HPA)																
C	1	0.01	0.00	0.00	0.00	0.00	-0.03	-0.03	-0.04	-0.04	-0.04	-0.04	-0.04	-0.04	-0.08	0.39
B	1	0.04	-0.08	-0.07	-0.04	0.01	0.00	-0.02	0.00	-0.03	-0.02	0.00	-0.05	-0.02	-0.05	0.37
N	1	0.04	0.07	0.06	0.04	-0.02	-0.07	-0.05	-0.08	-0.05	-0.07	-0.05	-0.02	-0.04	-0.11	0.39
C	2	0.01	0.01	0.01	0.00	0.00	-0.03	-0.03	-0.03	-0.03	-0.03	-0.04	-0.04	-0.04	-0.08	0.40
B	2	0.05	-0.08	-0.07	-0.04	0.01	0.00	-0.02	0.00	-0.03	-0.02	0.00	-0.05	-0.02	-0.05	0.38
N	2	0.05	0.07	0.07	0.04	-0.02	-0.07	-0.05	-0.08	-0.05	-0.07	-0.05	-0.02	-0.04	-0.11	0.40
Weinhold Natural Population Analysis (NPA)																
C	1	-0.03	-0.04	-0.06	-0.06	-0.08	-0.18	-0.18	-0.18	-0.19	-0.18	-0.18	-0.21	-0.21	-0.34	2.12
B	1	0.61	-0.39	-0.37	-0.26	-0.08	-0.09	-0.14	-0.11	-0.20	-0.17	-0.11	-0.25	-0.19	-0.29	2.05
N	1	-0.33	0.23	0.20	0.13	-0.13	-0.29	-0.25	-0.30	-0.23	-0.26	-0.20	-0.15	-0.20	-0.41	2.17
C	2	-0.02	-0.04	-0.06	-0.06	-0.08	-0.18	-0.18	-0.18	-0.19	-0.18	-0.18	-0.21	-0.21	-0.34	2.12
B	2	0.67	-0.41	-0.39	-0.28	-0.08	-0.10	-0.15	-0.12	-0.21	-0.18	-0.11	-0.25	-0.18	-0.29	2.06
N	2	-0.34	0.24	0.21	0.14	-0.13	-0.30	-0.26	-0.30	-0.23	-0.26	-0.20	-0.15	-0.20	-0.41	2.18
Merz-Kollman Electrostatic Potential Fit (ESP)																
C	1	-0.02	0.04	0.28	0.17	0.20	-0.19	-0.29	-0.35	-0.26	-0.23	-0.19	-0.08	-0.03	-0.51	1.48
B	1	0.24	-0.25	-0.07	0.03	0.24	0.02	-0.13	-0.09	-0.21	-0.13	-0.19	-0.23	-0.12	-0.43	1.32
N	1	0.25	0.06	0.16	0.15	0.15	-0.29	-0.31	-0.32	-0.30	-0.33	-0.15	-0.01	-0.07	-0.60	1.62
C	2	0.72	-0.27	0.01	-0.11	0.25	-0.10	-0.24	-0.29	-0.20	-0.19	-0.25	-0.16	-0.10	-0.50	1.51
B	2	0.96	-0.49	-0.27	-0.13	0.23	0.05	-0.12	-0.11	-0.22	-0.18	-0.18	-0.28	-0.14	-0.41	1.39
N	2	1.48	-0.46	-0.28	-0.32	0.25	-0.18	-0.25	-0.24	-0.21	-0.26	-0.23	-0.09	-0.16	-0.59	1.66

Table S10. Atomic charge (electron) distribution analysis upon single (n = 1) and double (n = 2) methane adsorption on MPh, B-MPh, and N-MPh determined by three conceptually different population analysis methods: Hirshfeld (HPA), Weinhold (NPA), and Merz-Kollman (ESP) at the MN15/def2-QZVPP level of theory. See **Figure 2** for a graphical plot and **Figure S1** for the numbering of atom positions (numbering of the second adsorbate is logical).

X	n	C25	proximal			distal	Σ CH ₄	C30	H31	proximal			distal	Σ CH ₄
			H26	H27	H28	H29				H32	H33	H34		
Hirshfeld Population Analysis (HPA)														
C	1	-0.13	0.02	0.02	0.02	0.03	-0.04							
B	1	-0.13	0.02	0.02	0.02	0.03	-0.03							
N	1	-0.13	0.02	0.02	0.02	0.03	-0.04							
C	2	-0.13	0.02	0.02	0.02	0.03	-0.03	-0.13	0.02	0.02	0.02	0.03	-0.03	
B	2	-0.13	0.02	0.03	0.02	0.03	-0.03	-0.13	0.02	0.03	0.02	0.03	-0.03	
N	2	-0.13	0.02	0.02	0.02	0.03	-0.04	-0.13	0.02	0.02	0.02	0.03	-0.04	
Weinhold Natural Population Analysis (NPA)														
C	1	-0.84	0.21	0.21	0.21	0.21	0.00							
B	1	-0.83	0.21	0.21	0.21	0.21	0.00							
N	1	-0.84	0.21	0.21	0.21	0.21	0.00							
C	2	-0.84	0.21	0.21	0.21	0.21	0.00	-0.84	0.21	0.21	0.21	0.21	0.00	
B	2	-0.83	0.21	0.21	0.21	0.21	0.00	-0.83	0.21	0.21	0.21	0.21	0.00	
N	2	-0.84	0.21	0.21	0.21	0.21	0.00	-0.84	0.21	0.21	0.21	0.21	0.00	
Merz-Kollman Electrostatic Potential Fit (ESP)														
C	1	-0.48	0.12	0.12	0.12	0.11	-0.01							
B	1	-0.50	0.12	0.13	0.13	0.11	0.00							
N	1	-0.50	0.13	0.12	0.12	0.12	-0.01							
C	2	-0.45	0.10	0.09	0.10	0.11	-0.05	-0.44	0.10	0.09	0.09	0.11	-0.05	
B	2	-0.46	0.09	0.10	0.10	0.12	-0.05	-0.46	0.09	0.10	0.10	0.12	-0.05	
N	2	-0.45	0.09	0.09	0.09	0.12	-0.06	-0.45	0.09	0.09	0.09	0.12	-0.06	

Table S11. Atomic spin densities of the adsorbent molecule for single (n = 1) and double (n = 2) methane adsorption on B-MPh and N-MPh from Hirshfeld population analysis (HPA) and Weinhold natural population analysis (NPA) at the MN15/def2-QZVPP level of theory. See **Figure S1** for the numbering of atom positions.

X	n	X1	β										γ	=CH ₂	Σ H	
			C2	α C3	C4	C5	C6	C7	C8	C9	C10	C11				C12
Hirshfeld Population Analysis (HPA)																
B	1	0.10	-0.01	0.05	0.18	-0.02	0.08	0.03	0.06	-0.02	-0.03	0.21	0.01	0.14	0.17	0.05
N	1	0.03	0.00	0.02	0.13	-0.01	0.11	0.07	0.09	0.02	0.00	0.15	-0.01	0.09	0.22	0.07
B	2	0.11	-0.01	0.05	0.18	-0.02	0.07	0.03	0.05	-0.03	-0.03	0.21	0.02	0.15	0.16	0.04
N	2	0.03	0.00	0.02	0.13	-0.01	0.11	0.07	0.09	0.02	0.00	0.15	-0.01	0.09	0.23	0.07
Weinhold Natural Population Analysis (NPA)																
B	1	0.11	-0.04	0.04	0.26	-0.08	0.11	0.04	0.06	-0.08	-0.10	0.30	-0.01	0.19	0.23	-0.03
N	1	0.03	-0.03	0.00	0.19	-0.08	0.17	0.10	0.12	-0.01	-0.06	0.22	-0.04	0.12	0.32	-0.04
B	2	0.11	-0.03	0.06	0.26	-0.08	0.10	0.03	0.04	-0.09	-0.10	0.30	0.01	0.21	0.22	-0.03
N	2	0.03	-0.03	0.00	0.18	-0.08	0.17	0.10	0.12	-0.01	-0.06	0.22	-0.04	0.11	0.32	-0.04

Table S12. Atomic spin densities of the adsorbate molecule(s) for single (n = 1) and double (n = 2) methane adsorption on B-MPh and N-MPh from Hirshfeld population analysis (HPA) and Weinhold natural population analysis (NPA) at the MN15/def2-QZVPP level of theory. See **Figure S1** for the numbering of atom positions (numbering of the second adsorbate is logical).

X	n	C25	proximal		H28	distal H29	Σ CH ₄	C30	H31	proximal		distal H34	Σ CH ₄
			H26	H27						H32	H33		
Hirshfeld Population Analysis (HPA)													
B	1	0.003	0.001	0.001	0.002	0.001	0.007						
N	1	0.001	0.001	0.001	0.001	0.000	0.003						
B	2	0.004	0.001	0.001	0.002	0.001	0.008	0.004	0.001	0.001	0.002	0.001	0.008
N	2	0.001	0.001	0.001	0.001	0.000	0.003	0.001	0.001	0.001	0.001	0.000	0.003
Weinhold Natural Population Analysis (NPA)													
B	1	0.001	0.000	0.000	0.000	0.001	0.002						
N	1	0.001	0.000	0.000	0.000	0.000	0.000						
B	2	0.001	0.000	0.000	0.000	0.001	0.002	0.001	0.000	0.000	0.000	0.001	0.002
N	2	0.000	0.000	0.000	0.000	0.000	0.000	0.001	0.000	0.000	0.000	0.000	0.000

Table S13. Thermochemical quantities (in kJ mol⁻¹) for comparison to experimental measurements of physisorptive binding of methane on porous carbon surfaces at 298 K. LoT: MN15/6-311++G**. MPh×CH₄ corresponds to 5.6 mmol g⁻¹ of absolute uptake and MPh×2CH₄ corresponds to 11.2 mmol g⁻¹, where uptake is defined as the true or “absolute” quantity. At room temperature (298 K), this corresponds to the following equilibrium pressures for adsorption on ZTC: 9.5 and 26.8 bar (or 9.3 and 26.4 atm), respectively. The enthalpy of desorption (ΔH) at these conditions is measured to be 13.5 and 13.1 kJ mol⁻¹, respectively (Stadie et al., 2015 – Reference 48).

System	P atm	$\Delta_{\text{des}}E^{\text{QM}*}$ kJ mol ⁻¹	$\Delta_{\text{des}}E_{\text{ZPE}}$ kJ mol ⁻¹	$\Delta_{\text{des}}U^{\text{SM}}$ kJ mol ⁻¹	$\Delta_{\text{des}}U^{\text{a}}$ kJ mol ⁻¹	$\Delta_{\text{des}}U^{\text{b}}$ kJ mol ⁻¹	$\Delta_{\text{des}}H^{\text{a}}$ kJ mol ⁻¹	$\Delta_{\text{des}}H^{\text{b}}$ kJ mol ⁻¹	$\Delta_{\text{des}}H^{\text{c}}$ kJ mol ⁻¹
MPh×CH ₄	1	14.8	-4.0	-7.4	7.4	10.8	9.8	13.2	17.2
B-MPh×CH ₄	1	13.9	-3.5	-7.2	6.6	10.4	9.1	12.9	16.4
N-MPh×CH ₄	1	17.4	-4.6	-7.6	9.8	12.9	12.3	15.3	19.9
MPh×CH ₄	9.3	14.8	-4.0	-7.4	7.4	10.8	9.8	13.2	17.2
B-MPh×CH ₄	9.3	13.9	-3.5	-7.2	6.6	10.4	9.1	12.9	16.4
N-MPh×CH ₄	9.3	17.4	-4.6	-7.6	9.8	12.9	12.3	15.3	19.9
MPh×2CH ₄	26.4	14.1	-4.1	-7.6	6.6	10.1	9.1	12.5	16.6
B-MPh×2CH ₄	26.4	13.4	-3.5	-7.3	6.1	9.9	8.6	12.4	15.9
N-MPh×2CH ₄	26.4	17.0	-4.4	-7.6	9.4	12.6	11.9	15.1	19.5

^a defined as $\Delta U^{\text{a}} = \Delta E^{\text{QM}*} + \Delta U^{\text{SM}}$ and $\Delta H^{\text{a}} = \Delta E^{\text{QM}*} + \Delta U^{\text{SM}} + RT$ referred to as ΔU° and ΔH° at P = 1 atm; ^b defined as $\Delta U^{\text{b}} = \Delta E^{\text{QM}*} + \Delta E_{\text{ZPE}}$ and $\Delta H^{\text{b}} = \Delta E^{\text{QM}*} + \Delta E_{\text{ZPE}} + \Delta PV$; ^c defined as $\Delta H^{\text{c}} = \Delta E^{\text{QM}*} + \Delta PV$

Table S14. Thermochemical quantities (in kJ mol⁻¹) for comparison to experimental measurements of physisorptive binding of methane on porous carbon surfaces at 298 K. LoT: MN15/def2-QZVPP. MPh×CH₄ corresponds to 5.6 mmol g⁻¹ of absolute uptake and MPh×2CH₄ corresponds to 11.2 mmol g⁻¹, where uptake is defined as the true or “absolute” quantity. At room temperature (298 K), this corresponds to the following equilibrium pressures for adsorption on ZTC: 9.5 and 26.8 bar (or 9.3 and 26.4 atm), respectively. The enthalpy of desorption ($\Delta_{\text{des}}H$) at these conditions is measured to be 13.5 and 13.1 kJ mol⁻¹, respectively (Stadie et al., 2015 – Reference 48).

System	P atm	$\Delta_{\text{des}}E^{\text{QM}*}$ kJ mol ⁻¹	$\Delta_{\text{des}}E_{\text{ZPE}}$ kJ mol ⁻¹	$\Delta_{\text{des}}U^{\text{SM}}$ kJ mol ⁻¹	$\Delta_{\text{des}}U^{\text{a}}$ kJ mol ⁻¹	$\Delta_{\text{des}}U^{\text{b}}$ kJ mol ⁻¹	$\Delta_{\text{des}}H^{\text{a}}$ kJ mol ⁻¹	$\Delta_{\text{des}}H^{\text{b}}$ kJ mol ⁻¹	$\Delta_{\text{des}}H^{\text{c}}$ kJ mol ⁻¹
MPh×CH ₄	1	13.6	-3.8	-7.4	6.1	9.8	8.6	12.2	16.0
B-MPh×CH ₄	1	13.1	-3.4	-7.3	5.8	9.7	8.3	12.2	15.6
N-MPh×CH ₄	1	16.1	-4.2	-7.5	8.6	11.9	11.0	14.4	18.6
MPh×CH ₄	9.3	13.6	-3.8	-7.4	6.1	9.8	8.6	12.2	16.0
B-MPh×CH ₄	9.3	13.1	-3.4	-7.3	5.8	9.7	8.3	12.2	15.6
N-MPh×CH ₄	9.3	16.1	-4.2	-7.5	8.6	11.9	11.0	14.4	18.6
MPh×2CH ₄	26.4	13.1	-3.6	-7.4	5.7	9.5	8.2	12.0	15.6
B-MPh×2CH ₄	26.4	12.8	-3.3	-7.3	5.5	9.5	8.0	12.0	15.2
N-MPh×2CH ₄	26.4	15.8	-4.1	-7.5	8.3	11.7	10.8	14.2	18.3

^a defined as $\Delta U^{\text{a}} = \Delta E^{\text{QM}*} + \Delta U^{\text{SM}}$ and $\Delta H^{\text{a}} = \Delta E^{\text{QM}*} + \Delta U^{\text{SM}} + RT$ referred to as ΔU° and ΔH° at P = 1 atm; ^b defined as $\Delta U^{\text{b}} = \Delta E^{\text{QM}*} + \Delta E_{\text{ZPE}}$ and $\Delta H^{\text{b}} = \Delta E^{\text{QM}*} + \Delta E_{\text{ZPE}} + \Delta PV$; ^c defined as $\Delta H^{\text{c}} = \Delta E^{\text{QM}*} + \Delta PV$

Table S15. Consequences of the gradual relaxation of the $\text{XC}_{47}\text{H}_{20}\times\text{CH}_4$ (i.e., blade $\times\text{CH}_4$ or X-blade $\times\text{CH}_4$, X = B or N), adsorption model structures on CH_4 binding energies in kJ mol^{-1} , as a function of site of interaction (C, B, or N). A number of stationary structures (N) below 28 indicates a ‘slip’ of CH_4 into an adjacent adsorption site than originally targeted. Basis sets used for MN15–, MN15, and MN15+ levels are 6-31G*, 6-311++G**, def2-QZVPP, respectively with the MN15 functional.

	N	average	std. dev.	minimum	maximum
<i>Relaxation of peripheral H, CH₄: MN15– level</i>					
blade $\times\text{CH}_4$	28	12.8	1.4	11	16
B-blade $\times\text{CH}_4$	28	12.7	1.5	11	16
N-blade $\times\text{CH}_4$	28	15.1	1.2	13	17
<i>Relaxation of peripheral H, CH₄, site of adsorption: MN15– level</i>					
blade $\times\text{CH}_4$	28	12.8	1.4	11	16
B-blade $\times\text{CH}_4$	28	12.8	1.6	10	16
N-blade $\times\text{CH}_4$	28	15.2	1.1	13	17
<i>Relaxation of peripheral H, CH₄, site of adsorption, α-carbons: MN15– level</i>					
blade $\times\text{CH}_4$	30	13.2	1.7	11	17
B-blade $\times\text{CH}_4$	26	12.9	1.6	11	16
N-blade $\times\text{CH}_4$	28	15.2	0.9	13	17
<i>Relaxation of peripheral H, CH₄, site of adsorption, α-carbons: MN15–/MN15 level</i>					
blade $\times\text{CH}_4$	30	17.7	1.9	14	21
B-blade $\times\text{CH}_4$	26	15.6	2.0	13	20
N-blade $\times\text{CH}_4$	28	18.9	1.3	16	21
<i>Relaxation of peripheral H, CH₄, site of adsorption, α-carbons: MN15 level</i>					
blade $\times\text{CH}_4$	30	17.8	1.9	14	21
B-blade $\times\text{CH}_4$	26	15.9	2.3	13	20
N-blade $\times\text{CH}_4$	28	19.0	1.3	16	21
<i>Relaxation of peripheral H, CH₄, site of adsorption, α-carbons: MN15/MN15+ level</i>					
blade $\times\text{CH}_4$	30	13.8	1.7	11	17
B-blade $\times\text{CH}_4$	26	12.9	1.7	10	15
N-blade $\times\text{CH}_4$	28	15.3	1.1	14	17